

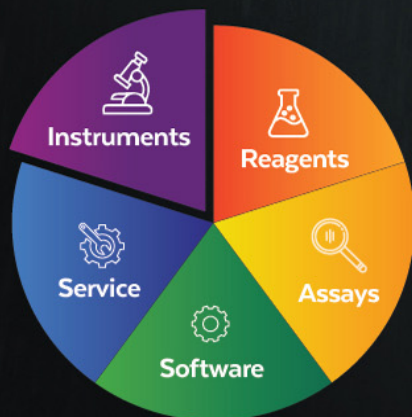
EMPOWERING YOUR DISCOVERY

COMPLETE SINGLE-CELL DATA FROM EASY WORKFLOWS

Now you too can collect and analyze more emitted light from each fluorochrome. The Cytex® Northern Lights™ system was designed with **easy-to-use workflows, assay flexibility, and improved sensitivity** in mind. Empower your flow cytometry research with Full Spectrum Profiling™ technology.

- **Maximum flexibility** when designing panels and choosing fluorochromes
- **Easy instrument setup** with Cytex Assay Settings
- **Standardized instrument setup** with automated daily QC
- **Store and re-use reference controls**, saving time and reagent costs

READY TO GET STARTED?



https://welcome.cytexbio.com/ez_spectral

Therapeutic antibody glycosylation impacts antigen recognition and immunogenicity

Babette Wolf¹, Mateusz Piksa¹, Isabelle Beley¹, Agnes Patoux¹, Thierry Besson¹, Valerie Cordier¹, Bernd Voedisch¹, Patrick Schindler¹, Daniela Stöllner¹, Ludovic Perrot¹, Stephan von Gunten², Dominique Brees¹, Michael Kammüller¹

¹Novartis Institutes for BioMedical Research, Basel, Switzerland

²Institute of Pharmacology, University of Bern, Bern, Switzerland

babette.wolf@novartis.com
mateusz.piksa@novartis.com
isabelle.beley@novartis.com
agnes.patoux@novartis.com
thierry.besson@novartis.com
valerie.cordier@novartis.com
bernd.voedisch@novartis.com
patrick.schindler@novartis.com
daniela.stollner@novartis.com
ludovic.perrot@novartis.com
stephan.vongunten@pki.unibe.ch
dominique.brees@novartis.com
michael.kammüller@novartis.com

Keywords: Antigen Presentation/Processing, Antibodies, Tolerance, Fc receptors

Abbreviations: ADA: anti-drug antibody, APC: antigen presenting cell, CHO: chinese hamster ovary, DC-SIGN: dendritic cell-specific ICAM-3 grabbing non-integrin, Fuc: fucose, Gal: galactose, GlcNAc: N-acetylglucosamine, IDC: immature dendritic cell, IG: immunogenicity, LR: lectin receptor, MR: mannose receptor, Neu5Ac: N-Acetyl-neuraminic acid, Neu5Gc: N-Glycolyl-neuraminic acid, RTX: rituximab, WT: unmodified, HiMan: mannosylated, HySi: hypersialylated, N297A: aglycosylated, Siglec: sialic acid-binding Ig-like lectin, SI: stimulation index, RI: response index

This work involving animals has been conducted according to the authorized study protocol (approved by the Novartis Animal Care and Use Committee) and local standard operating procedures in strict compliance with national legal regulations on animal welfare law and accepted animal welfare standards. Work involving human blood was conducted upon receipt of written, informed consent in accordance to the international ethical standards defined by the Declaration of Helsinki.

This article has been accepted for publication and undergone full peer review but has not been through the copyediting, typesetting, pagination and proofreading process which may lead to differences between this version and the [Version of Record](#). Please cite this article as doi: [10.1111/imm.13481](https://doi.org/10.1111/imm.13481)

Summary

Here we demonstrate that antibody glycosylation impacts antigen recognition and immunogenicity. Fc glycans facilitate the efficient uptake of antibodies in a receptor-dependent manner by DCs, and thus determine routing, processing, presentation and ultimately humoral responses. Engineering of Fc glycosylation to high mannose type increases and to sialylated complex type decreases DC-uptake and effector T cell responses.

Abstract

In this study we show that glycosylation is relevant for immune recognition of therapeutic antibodies, and that defined glycan structures can modulate immunogenicity. Concerns regarding immunogenicity arise from the high heterogeneity in glycosylation that is difficult to control and can deviate from human glycosylation if produced in non-human cell lines. While non-human glycosylation is thought to cause hypersensitivity reactions and immunogenicity, less is known about effects of Fc-associated glycan structures on immune cell responses. We postulated that glycosylation influences antigen recognition and subsequently humoral responses to therapeutic antibodies by modulating 1) recognition and uptake by dendritic cells (DCs), and 2) antigen routing, processing and presentation. Here, we compared different glycosylation variants of the antibody rituximab (RTX) in *in vitro* assays using human DCs and T cells as well as in *in vivo* studies. We found that human DCs bind and internalize unmodified RTX stronger compared to its aglycosylated form suggesting that glycosylation mediates uptake after recognition by glycan-specific receptors. Furthermore, we show that DC-uptake of RTX increases or decreases if glycosylation is selectively modified to recognize activating (by mannosylation) or inhibitory lectin receptors (by sialylation). Moreover, glycosylation seems to influence antigen presentation by DCs because specific glycovariants tend to induce either stronger or weaker T cell activation. Finally, we demonstrate that antibody glycosylation impacts anti-drug antibody (ADA) responses to RTX *in vivo*. Hence, defined glycan structures can modulate immune recognition and alter ADA responses. Glyco-engineering may help to decrease clinical immunogenicity and ADA-associated adverse events such as hypersensitivity reactions.

Introduction

Antibody therapeutics are among the fastest growing medicinal drug classes and are used to treat a variety of diseases such as cancer, autoimmune and infectious diseases. They are highly specific, thus expected to offer safer treatment options compared to small molecular weight drugs. Nevertheless, therapeutic proteins may be prone to cellular and humoral immunogenic responses by the patient's immune system. Clinically, immunogenicity is usually characterized by the presence of anti-drug antibodies (ADAs). The formation of ADAs typically requires recognition and uptake by dendritic cells (DCs), the most proficient antigen presenting cells of the immune system. These cells process antigens into peptides which are presented in the context of major histocompatibility (MHC) class II receptors to helper T cells (Th). With adequate co-stimulatory signals, activated Th cells provide cognate help to B cells allowing plasma cells to differentiate and to secrete highly specific antibodies directed against the antigen, hence leading to the formation of ADAs. ADAs that bind to the target binding site of the therapeutic protein are called neutralizing antibodies. In addition, even non-neutralizing antibodies may cause clinical issues as ADA-protein complexes can be cleared faster. Overall, these events can lead to diminished efficacy but also cause hypersensitivity reactions ranging from mild (skin rash, fever, hypotension, urticaria, serum sickness) to acute severe (anaphylaxis) outcomes.

In order to avoid immunogenicity, it is crucial to understand contributing risk factors. Immunogenicity is the result of converging drug, treatment and patient factors. Glycosylation is one potential known drug-related risk factor among several others.

Antibodies of the IgG isotype contain a conserved glycosylation site which is an asparagine at position 297 in the CH2 domain providing the template for N-linked glycosylation and here called Fc glycan. Although the percentage of Fc glycosylation is low (2 – 3 % relative to the total mass of the molecule), subtle changes in Fc glycosylation can greatly impact Fc effector function, clearance and IgG-mediated inflammation.

Two aspects need to be distinguished as potential cause for glycosylation-mediated immunogenicity: 1) non-human glycosylation and 2) glycan heterogeneity. Most therapeutic antibodies are produced in non-human cell lines such as chinese hamster ovary (CHO) or mouse myeloma cells (NS0; SP2/0). Therefore, non-human glycan

Accepted Article

structures can be incorporated and constitute a concern. Such human-foreign glycosylation patterns can induce immune responses as demonstrated by the presence of anti-glycan antibodies in human serum. Typical non-human glycans synthesized by above-mentioned cell lines are α 1-3gal (Gal α 1-3Gal β 1-4GlcNAc extension) and N-glycolylneuraminic acid (Neu5Gc), the non-human version of sialic acid. A prominent example where α 1-3gal and Neu5Gc containing glycans can cause severe hypersensitivity reactions, i.e. anaphylactic shock, is cetuximab which is produced in murine myeloma SP2/0. Pre-existing IgE antibodies reacting with Fab-associated α 1-3gal epitopes cause these severe side effects (1). A role of Neu5Gc in cetuximab-induced anaphylaxis could also be confirmed if located in the Fab-associated glycan (2). Interestingly, also Fc-associated Neu5Gc can be recognized by anti-Neu5Gc but only if at least two Neu5Gc are present (3).

Glycan heterogeneity is the second concern because of the distinct effects of certain glycan species on Fc effector function. Heterogeneity arises from the presence and activity of glycosyltransferases and glycosidases which determine the substrate (i.e., monosaccharide) specificity and linkage type. The core structure of the mature antibody Fc glycan is formed by a hepta-saccharide composed of two consecutive GlcNAc residues conjugated to a tri-mannose that is the starting point for two branches and extended by the addition of one GlcNAc on each branch. With addition of galactose, sialic acid and fucose the glycan structure of this complex type glycans can be elongated in a variety of possibilities which cause structural heterogeneity. Of note, the glycans on each IgG heavy chain may not be identical which introduces further heterogeneity. For example, in human serum IgG, up to 30 different glycovariants have been detected (4). The majority of the antibody Fc glycans are complex type glycans. The immature high mannose and hybrid type glycans typically occur only in low amounts (0.1 and 0.6 %, respectively, relative to the total mass of the glycans).

In therapeutic monoclonal antibodies the glycosylation pattern is a critical quality attribute because specific glycans are relevant for the functional activity but may also impact immunogenicity. Glycosylation patterns on therapeutic antibodies produced in mouse myeloma or CHO can vary (5). Therefore, a switch from one expression host system to another is not advisable. Because these cells do not entirely express the glycosylation machinery needed to produce human glycosylation, the glycan pattern slightly differs from

that generated by human cells. Another complicating factor is that the glycosylation patterns of therapeutic proteins are highly dependent on the expression and culture conditions (6). For Rituximab (RTX), a process change in the manufacturing in CHO resulted in an increase in afucosylated glycans which enhanced ADCC activity (7). Immature high mannose glycans usually only occur in low amounts in therapeutic antibodies. However, switching to high productivity mode during expression was reported to increase the proportion of high mannose structures which could affect the clearance (5). In addition, high mannose glycans may be recognized by lectin receptors (LR) which are expressed by DCs. Recognition of high mannose glycans exposed on therapeutic proteins by DCs has already been demonstrated. For example, exposed oligomannose on human coagulation FVIII was shown to increase internalization by APCs and linked to immunogenicity (8). However, glycan structures on therapeutic proteins differ from that on an antibody Fc. First, complex tri- or tetra-antennary glycans are common on therapeutic proteins as opposed to mono and bi-antennary glycans in Fc glycans (9, 10). Second, therapeutic protein glycans are less sialylated but more mannosylated. Third, therapeutic protein glycans are exposed on the surface compared to the Fc glycans which are thought to be buried and less accessible (11, 12). Fourth, the proportion of glycosylation is higher on therapeutic proteins compared to therapeutic antibodies. Finally, O-glycosylation sites are present in therapeutic proteins but absent in therapeutic antibodies. For example, erythropoietin (Epo) has 3 N- and 1 O-glycosylation site(s). Because the molecular weight of Epo (34 – 38 kDa) is low compared to an antibody (150 kDa) the relative glycan proportion is high (40 % vs 2 – 3 %, (13). For these reasons the theoretical risk that Fc glycans can affect immunogenicity appears to be low. However, to date, no clear evidence exists that Fc glycans do or do not contribute to immunogenicity.

In addition, it is not known whether deviations in glycan composition from that found on human serum IgGs affect immunogenicity. By 2012 16 mAbs engineered to contain decreased fucose content have entered clinical testing (14). These preclinical and clinical studies did not indicate that glycan modification increases the immunogenicity risk. Since no direct head-to-head comparison of the glyco-modified vs unmodified mAbs is done in the clinical setting the possibility that glycan modification impacts immunogenicity cannot be excluded. In addition, so far, no more than two glyco-engineered antibodies (Obinutuzumab and Mogamulizumab) have been approved (<https://www.antibodysociety.org/resources/approved-antibodies/>). Thus, currently, there

is insufficient conclusive evidence concerning the role of antibody glycosylation for antigen recognition and immunogenicity. It may be possible that the increased engagement of FcγRs by afucosylated antibodies increases the activation state of FcγR expressing cells, including APCs, thus promoting pro-inflammatory conditions that may contribute to antigen recognition and in turn cause immunogenicity. In addition, not only changes in fucose but also in galactose, mannose or sialic acid content could likewise affect immunogenicity. Indeed, Reusch and Tejada (15) concluded that the effect of these antibody Fc glycans on immunogenicity is unknown. One study showed an effect of galactose/GlcNAc on human serum IgG on the recognition by APCs where agalactosylated IgG increased DC uptake due to GlcNAc exposure (16). To date no evidence has been provided on whether changes in mannose/sialic acid and galactose content impact immunogenicity of therapeutic antibodies.

To gain more insights on the relevance of antibody glycosylation for antigen recognition and on immunogenicity, we used the commercially available therapeutic antibody RTX (a chimeric anti-CD20 hlgG1) to obtain several specific glycovariants, as RTX is associated with ADA formation in treated patients (17-19). We compared an aglycosylated RTX (N297A) with the inherently glycosylated RTX (WT) in order to probe whether glycosylation increases immune responses. Furthermore, we engineered RTX glycosylation to contain mainly pre-mature high mannose glycans (thus called HiMan) or terminating in α 2-6Neu5Ac (thus called HySi). We investigated whether these HiMan and HySi modifications promote immunogenic or tolerogenic effects, respectively. To get insights on the mechanism of glycosylation-related immunogenicity we conducted *in vitro* experiments using human monocyte-derived dendritic cells (moDCs) and T cells. Experiments covered glycosylation-dependent DC recognition and internalization upon LRs/FcγR/Siglec blockade, routing into to the endolysosomal compartment and T cell responses. Finally, we assessed the effect of antibody glycosylation on the humoral immune response *in vivo* in BALB/c mice.

Materials and Methods

1. RTX glycovariants

Rituximab is a chimeric m/hlgG1k monoclonal antibody targeting human CD20. It is approved for the treatment of rheumatoid arthritis, systemic vasculitis and B cell lymphoma. It has been selected as tool antibody because it is associated with a high incidence of clinical immunogenicity up to 65 % (17).

Expression vector harboring heavy and light chain, neomycin resistance, and recombinant DHFR gene was constructed at GeneArt (Life Technologies). Rituximab glycovariants were expressed in CHO cell lines as summarized in Table 1 except for the aglycosylated N297A (single point mutation of asparagine (N) to alanine (A) leads to loss of the conserved N-glycosylation site) which was produced in HEK293.

Host CHO cell line was cultivated in a proprietary medium A in T-flasks and incubated at 37°C and 5 % CO₂. For the generation of the stable cell line, the host CHO cell line was transfected with the linearized mAb-expressing vector using Cell line Nucleofection kit V (Lonza) and Nucleofector™ 2b (Lonza) device, according to the manufacturer's protocol. After the transfection, the antibiotic selection was performed, followed by MTX amplification. Single-cell cloning was performed by limited dilution in 96-well plates with a proprietary medium B. Single cells were expanded and cultured in shake flasks with proprietary medium B.

For HiMan, an α -mannosidase inhibitor kifunensine (Sigma #K1150) was added at 5 μ M at the start of the culture in order to inhibit N-glycan maturation. HySi was produced in a CHO cell line transfected with genes encoding β 1-4galactosyltransferase, CMP-sialic acid transporter and α 2-6-sialyltransferase. The antibodies were purified using Protein A chromatography followed by size-exclusion chromatography. For HySi, ConA purification was done to remove contaminations of high mannose glycans found after expression in CHO HySi cell line which has also been observed by others (20).

The final material was tested for purity by SDS-polyacrylamide gel electrophoresis which shows purity above 95 % i.e. aggregates below 5 % (Table 1). The antibody sequence was verified by mass spectrometry. Aggregation was analyzed by size exclusion chromatography coupled with multi-angle light scattering detector (SEC-MALS). Endotoxin content was determined by limulus amoebocyte lysate cartridges from Charles

River (Endosafe®).

Variant	WT	HiMan	HySi	N297A
Cell line	CHO-HPT1	CHO-HPT1 + kifunensine	CHO HySi	HEK293-6E
Endotoxin (EU/mg)	<0.07	<0.07	<0.25	<0.07
Aggregation (%)	0.41	0.25	0	0.7

Table 1: Overview of RTX glycovariant expression, purification and analytics

2. Glycan analysis

Glycan analysis for all glycovariants except for N297A was performed by LC-MS (liquid chromatography-mass spectrometry) by intact mass measurement after FabRICATOR (IdeS: streptococcal Ig-degrading enzyme, Genovis) treatment of the antibody samples which generates F(ab')₂ and two Fc fragments by cleavage in the hinge region. FabRICATOR cleavage was done by 1 h incubation of 1 µL of FabRICATOR (0.67 U/unit) per 2.5 µg of RTX which had been dried before using SpeedVac and re-suspended in 10 µL PBS at 37°C. After FabRICATOR cleavage, reduction of disulfide bonds was performed by adding 40 µL of 8 M urea / 0.4 M NH₄HCO₃ and 2 µL of DTT 1 M and incubated at 50°C for 30 min. Then 0.05 µg of the treated sample has been injected and analyzed by LC-MS. LC-MS analyses were performed using a SYNAPT G2S QTOF mass spectrometer (WATERS) coupled with an UPLC (ACQUITY I class, WATERS). A Bioresolve column (2.7 µm, 1×50 mm, WATERS) was used for mAb subunit (i.e. LC, Fc and Fc/2) separation. An elution gradient with mobile phase A (0.1 % formic acid in water) and mobile phase B (0.1 % formic acid in acetonitrile) was generated using the following program: 1) isocratic at 5 % B for 1.5 min; 2) linear gradient from 5 to 25 % B from 1.5 to 2 min; 3) linear gradient from 25 to 50 % B from 2 to 12 min; 4) linear gradient from 50 to 95 % B from 12 to 13 min; 5) isocratic at 95 % B from 13 to 15 min; 5) linear gradient from 95 to 5 % B from 15 to 15.5 min; and finally 6) isocratic at 5 % B from 15.5 to 20 min. The mass spectrometer was working in positive resolution mode and calibrated with NaCl 2 mg/mL. MS trace was acquired at mass range m/z 600 – 4500, 1 sec scan time, 3 kV capillary voltage, 40 V cone voltage, 350 °C desolvation temperature and 50 L/h cone gas flow. In addition, a UV trace was acquired at a wavelength of 214 nm.

Co-eluted multiple charged Fc/2 glycoforms were combined and deconvoluted using MassLynx MaxEnt1 algorithm (WATERS) to obtain measured average masses. Attribution of the different glycoforms was done by measuring the difference between the

calculated mass based on the amino acid sequence and the measured masses (**Table 2**). The relative percentage of each glycoform has been calculated by using the intensity of each corresponding deconvoluted ion signal.

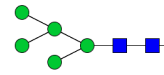
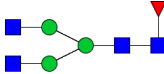
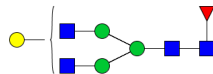

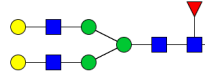
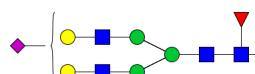
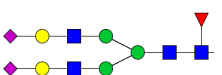
Name (Oxford)	Average Mass difference (Da)	Structure
M5 (M5)	1217.1	
G0F (FA2)	1445.3	
G1F (FA2G1)	1607.5	
G1FS1 (FA2G1S1)	1898.7	
G2F (FA2G2)	1769.6	
G2FS1 (FA2G2S1)	2060.9	
G2FS2 (FA2G2S2)	2352.1	

Table 2: MS based glycan attribution based on mass differences

Sialic acid linkage analysis was conducted using sialidases specific for α 2-3-linkage (Sialidase S from Prozyme and SialEXO 23 from Genovis). Sialic acid content of HySi did not decline after treatment with these α 2-3-specific sialidases and confirms exclusive α 2-6 linkage of HySi sialoglycans.

Glycan profiles for G1m17,1 allotype RTX glycovariants are depicted in Supplementary Figure 1. WT is characteristic of abundant fucosylated mono-galacto (G1F: 54.1 %), fucosylated agalacto (G0F: 30.1 %) and fucosylated di-galacto (G2F: 14.1 %) species and is therefore overall comparable to the EU-marketed rituximab (MabThera) with some minor deviations. One has to consider that glycosylation patterns can be influenced by minor changes in the manufacturing process, thus can lead to batch-to-batch variations

which is also reported for MabThera (7). In line with that, there is some variation in the proportion of high mannose and sialylation in MabThera depending on the report ranging from 1.43 % – 5.2 % and 0.98 % – 2.4 %, respectively (21-23). The observed proportion of 1.7 % M7 species found in RTX WT lies within this range while sialylation content is 0 %. In addition, our RTX WT contains a slightly higher percentage of total galactosylation (46.2 % – 51.1 % for MabThera vs 68.2 % for RTX WT). Such minor deviations are also reported for biosimilar products of rituximab. In order to exclude that such differences in the glycosylation pattern impact the efficacy and safety it is crucial that biosimilar manufacturers demonstrate equivalence to the originator product. The main purpose of the current study was to demonstrate that specific glycans i.e., mannose and sialic acid species contribute to RTX' immunogenic or tolerogenic properties, respectively. The WT RTX was for this purpose compared with highly mannosylated RTX (HiMan) and highly sialylated RTX (HySi) which differ remarkably in the glycosylation pattern as shown in Supplementary Figure 1. Therefore, we don't consider the minor deviations in the glycosylation pattern of our RTX WT from MabThera as relevant for the interpretation of the results.

The HiMan glycan profile is dominated by mannose 9 (M9: 74.3 %) and mannose 8 (M8: 21.6 %) species and minor mannose 7 (M7: 4.1 %) species. The HySi (total sialic acid: 89.7 %) accumulates fucosylated di-sialo-di-galacto (G2FS2: 41.6 %), fucosylated mono-sialo-di-galacto (G2FS1: 34.3 %), fucosylated mono-sialo-mono-galacto (G1FS1: 11 %) and mono-sialo-di-galacto (G2S1: 2.9 %) species.

3. Lectin ELISA

Lectin ELISA (enzyme-linked immunosorbent assay) was conducted to assess whether antibody Fc N-glycans are accessible to plant lectins. Coating of WT and N297A was done in 96 well plates (NUNC, Immunoplate Maxisorb) at 3 µg/mL followed by blockade with Carbo-Free blocking solution (Vectorlab, #SP-5040). Binding to biotinylated lectins (*Rhizinus communis* agglutinin, Concanavalin A, *Datura stramonium* lectin, *Aleuria Aurantia* lectin all from Vectorlab) was assessed at 10 µg/mL in HEPES-based buffer + 0.1 mM Ca²⁺ with (200 mM) or without inhibiting monosaccharides (D-galactose, α-methylmannoside, all from Vectorlab) and detected after incubation of HRP-conjugated streptavidin (Jackson Immunoresearch) and subsequent determination of TMB-derived

colorimetric signal using a spectrophotometer (Spectramax, Molecular Devices) and reported as optical density (OD).

4. Generation of immature DCs (IDCs)

Monocytes were isolated from buffy coats (24 – 72h after collection) according to the manufacturer's recommendation using the StraightFrom[®] Buffy Coat CD14 MicroBead Kit (Miltenyi, #130-114-976) on the MultiMACS[™] Cell24 Separator Plus system (Miltenyi). CPD (Citrat-Phosphat-Dextrose) buffered buffy coats were collected from healthy humans by leukapheresis in the blood donation center Bern, Switzerland according to local ethical regulations. Monocyte purity was confirmed by flow cytometry (Attune NxT, Thermo Scientific[™]) with >90 % CD14⁺ cells using the MACS Control MC CD14 Monocyte Cocktail (Miltenyi, # 130-092-859, cocktail of CD45-VioBlue, CD15-APC and CD14-PE). Isolated monocytes were differentiated to immature dendritic cells (IDCs) in human Mo-DC Differentiation Medium (Miltenyi, #130-094-812) or in RPMI1640 (Gibco, #21875) + 10 % heat-inactivated FBS (Gibco) + 1mM HEPES (Gibco, #15630-056) + 1 mM sodium pyruvate (Gibco, # 11360070) + 1 x NEAA (non-essential amino acids, Gibco, #11140-050) + 1 % P/S (Gibco, #15070-063) + 1000 U IL-4 (Miltenyi, #130-093-924) + 1000 U GM-CSF (Miltenyi, #130-093-868) for 5 – 6 days at $1 - 2.5 \times 10^6$ cells/mL, 37°C and 5 % CO₂. Mo-DC Differentiation Medium was replenished on day 3 or 4.

5. Phenotypic characterization of IDCs

Differentiation status and LR/FcγR expression was determined for each donor by flow cytometry (Attune NxT) using 1×10^5 IDCs per sample. Matched isotype controls were used to account for residual Fc-mediated binding of surface marker antibodies. Antibodies for CD206 (R&D, #MAB25342), DCIR (R&D, #MAB1748), DC-SIGN (R&D, #MAB161), DEC-205 (R&D, #MAB20471), Siglec 7, (R&D, #MAB1138), FcγRI (Biolegend, #305016), FcγRII (Biolegend, #557333), FcγRIII (Biolegend, #302014) were conjugated to Alexa Fluor 488 using the Antibody labeling kit AF488 from Thermo Scientific[™] (#A20181). The labeling degree was evaluated on a Nanodrop 8000 Spectrophotometer (Thermo Scientific[™]). Differentiation status was assessed by staining for CD11c (Beckman Coulter, #IM3707), CD14 (Beckman Coulter, #IM27074) and CD1a (Becton Dickinson, #559775).

6. Internalization assay

6.1. Indirect FACS assay

IDCs (1.5×10^5 per sample) were incubated with 10 $\mu\text{g}/\text{mL}$ unlabeled RTX glycovariants in binding buffer (HBS (Hepes-buffered saline) + 1 mM CaCl_2 , 1 mM MgCl_2 , 1 mM MnCl_2) at 4°C (for binding) or 37°C (for internalization) for 15, 30, 60 and 120 min. IDCs were washed to remove excess free RTX. Then, the residual amount of surface-bound RTX was detected using 10 $\mu\text{g}/\text{mL}$ FITC-labelled anti-RTX (Biorad, #MCA2260F). After another wash step, stained IDCs were fixed (1 % paraformaldehyde) and measured on the Attune NxT flow cytometer. Staining of CD20⁺ Ramos cells was performed initially to confirm that the indirect staining protocol is valid and that RTX glycovariants bind equally to CD20.

For inhibition experiments, IDCs were pre-incubated for 30 min at 4°C with the respective blocking agents anti-CD32 F(ab')₂ (Ancell, #181-520), Fc blocking reagent (Miltenyi, #120-000-442) and Mannan (Sigma, #M7504-250) before addition of unlabeled RTX glycovariants.

The difference of the 4° and 37°C fluorescence signal was calculated and scaled using the plogis() function in R and expressed as percentage of internalization.

6.2. IncuCyte® Internalization Assay

An orthogonal method to measure internalization by IDCs was established using the IncuCyte® Live cell Image Analyser (Sartorius). The principle is based on the detection of intracellular fluorescence signals resulting from internalization of fluorochrome-labeled RTX glycovariants. Fluorochrome conjugation was done using the Antibody labeling kit AF647 from Thermo Scientific™ (#A20186) according to the manufacturer's protocol. The labeling degree for all RTX glycovariants was comparable with 5 – 6 mole AF647 per mole RTX as determined by absorption at 280 nm and at 650 nm on the Nanodrop (Thermo Scientific™).

IDCs were seeded into a transparent flat bottom 96 well plate (Nunc, #3595) at $1 \times 10^5/\text{well}/100 \mu\text{L}$ in Mo-DC Differentiation Medium (Miltenyi, #130-094-812) and incubated over night at 37°C and 5 % CO_2 . On the next day, the medium was replaced by medium (RPMI1640 + 1mM Hepes + 1 mM sodium pyruvate + 1 mM NEAA + 1 mM MgCl_2 + 1 mM CaCl_2 + 1 mM MnCl_2) containing 10 $\mu\text{g}/\text{mL}$ AF647-conjugated RTX glycovariant after the plate was kept for 10 min in the fridge. After 30 min incubation in the fridge, the

supernatant was replaced by warm medium (RPMI1640 + 1mM Hepes + 1 mM sodium pyruvate + 1 mM Glutamax + 1 mM NEAA) and placed immediately into the IncuCyte analyser. Images were acquired at 20x magnification every 20 min for the first 5 h and every hour for up to 24 h.

Inhibition experiments included an intermittent incubation step in the fridge for 30 min before addition of RTX fluorochrome conjugates. Following inhibitors were tested: rhu (recombinant human) Siglec 7 (Biorbyt, #orb428446), rhu DC-SIGN (R&D, #9136-DC), rhu MR (R&D, #2534-MR/CF), Mannan (Sigma, #M7504-250).

Internalization was determined from quantification of intracellular fluorescence. Hereto, masks were created on phase and fluorescent objects using the Basic analyzer mode to capture IDCs and internalized RTX, respectively. Integrated Intensity (RCU x μm^2) per well was reported.

7. Confocal imaging

In order to determine into which intracellular compartment RTX is routed after internalization confocal laser scanning microscopy was utilized. IDCs were seeded at 3×10^5 cells in 300 μL Mo-DC Differentiation Medium (Miltenyi, #130-094-812) per chamber of an 8 well chamber slide (Corning, #354108) and incubated over night at 37°C and 5 % CO₂. On the next day, medium was replaced by binding buffer (HBS + 1 mM CaCl₂, 1 mM MgCl₂, 1 mM MnCl₂) containing 20 $\mu\text{g}/\text{mL}$ AF647-conjugates of RTX glycovariants and incubated for 120 min at 4°C (fridge) and 37°C and 5 % CO₂. IDCs were fixed (4 % paraformaldehyde) and permeabilized (0.1 % Triton X-100 in PBS). After a blocking step with 2 % BSA in PBS IDCs were incubated with marker antibodies for LAMP-1 (Sigma, #L1418), EEA1 (Abcam, #ab109110) and Rab7 (Abcam, #ab137029) followed by the secondary donkey anti-rabbit-AF488 (LifeTech, #A-21206 1:1000 dilution). DAPI (4',6-diamidino-2-phenylindole) was added as nuclear stain. Stained IDCs were mounted in FluoSafe reagent (Calbiochem, # 345789) and covered with a glass slide. Cured slides were imaged on an Olympus FV3000 at 40x magnification.

Quantification of internalized RTX was done using HALO™ image analysis software (Akoya Biosciences) by determination of percentage of AF647-positive area per image. The number of IDCs per image was constant for all tested conditions (n = ~120 per image).

8. T cell assay

PBMCs (peripheral blood mononuclear cells) were isolated from buffy coats donated by naïve human subjects at blood donation center in Bern according to local ethical practices. Briefly, 1:2 PBS-diluted buffy coats were added to Leucosep™ tubes (Greiner, #227289) containing Biocoll (Biochrome, #L6115). The white PBMC layer was collected after density gradient centrifugation for 15 min at 980 g without brake. PBMCs were washed (centrifugation at 360 g, 4°C 15 min), platelets removed by centrifugation at 200 g for 10 min at 4°C. Isolated PBMCs were stained with 5 µM CellTrace™ Violet (CTVio, LifeTech, #C34557) for 20 min in a water bath (37°C). Excess CTVio was removed after 5 min (RT) incubation of CTVio-incorporated cells with platelet-free autologous plasma by centrifugation at 360 g for 5 min. CTVio-negative PBMCs were used as control for compensation and as FMO (fluorescence minus one) control. CTVio⁺ PBMCs were seeded at 1×10^6 cells/mL into 24 well plates (Nunc, #142475) in X-Vivo (Lonza, #BE02-060F) + 5 % platelet-free autologous plasma and stimulated (primed) with 1 and 10 µg/mL of the respective RTX glycovariant, 5 - 30 µg/mL KLH (keyhole limpet hemocyanin, Thermo Scientific™, #77600), 0.5 µg/mL Tetanus toxoid (TT, Enzo, #ALX-630-108) or medium for 5 days. An aliquot of the buffy coat was used to isolate monocytes and differentiate to IDCs as described in Method section 4. On day 5, DC-PBMC co-culture (1:10) was re-stimulated (challenged) with 1 and 10 µg/mL RTX glycovariants, 5 - 30 µg/mL KLH, 0.5 µg/mL TT or medium and incubated for 4 additional days in presence of 5 U/mL IL-2 (Roche, #11011456001). On day 9, stimulated cells were harvested and stained with the surface markers CD3 (Beckman Coulter, #A07749), CD4 (Becton Dickinson, #560158), CD25 (Becton Dickinson, #555434) including a viability dye (Zombie aqua, Biolegend, #423102). Stained cells were measured on the Attune NxT flow cytometer using constant volumetric stop condition for all samples. FMO controls were used to discriminate between positive and negative populations. Absolute counts of proliferating and activated T_h cells were determined after priming and challenging and expressed as stimulation index (SI) indicating the challenge response relative to the priming response. Donors showing an SI above 1.5 were assigned as T cell responders.

9. Immunogenicity to RTX in mice

9.1. Study design

Animal studies were performed according to the federal and cantonal law of Switzerland and under licenses approved by the Cantonal Veterinary Office of Basel Stadt, Switzerland. Three different studies were conducted. In the first study (strain comparison), a protocol suitable to induce a robust immune response to RTX was established where C57BL/6 and BALB/c mice were compared. In the 2nd study (IG study) glycosylation-related immunogenicity was assessed in BALB/c mice. In the last study (IG study with adjuvant), immunizations of BALB/c mice were performed in conjunction with the adjuvant alum to assess glycosylation-dependent *ex vivo* recall CD4⁺ T cell responses.

Strain comparison study:

Male BALB/c mice (BALB/cAnNCrl, from Charles River) and male C57BL/6J (from Jackson Laboratory) with an age of 10 weeks and 10 animals per group were dosed subcutaneously (2 x next to the inguinal region of the abdomen) twice weekly 8 x on D1, D4, D8, D11, D15, D18, D22 and D55 with 0.5 mg/kg of RTX glycovariants or vehicle control (PBS). IG samples were collected prior the start of the study on -D7, pre-dose on D11, D15, D18, D22, D55 and at necropsy on D60. PK samples were collected prior the start of the study on -D7 and on D55 (4h post dose). Hereto, whole blood was collected from the saphenous vein into serum separation tubes and stored at room temperature for at least 30 min. After 10 min centrifugation at ~2,000 x g, serum was collected and frozen at -80° C.

IG study:

Male BALB/c mice (BALB/cAnNCrl, from Charles River, age of 9 weeks, 10 animals per group) were dosed subcutaneously (2 x next to the inguinal region of the abdomen) twice weekly 6 x on D1, D4, D8, D11, D15 and D18 with 0.5 mg/kg of RTX glycovariants or vehicle control (PBS). IG samples were collected prior to the start of the study on -D13 and pre-dose on D4, D8, D11, D15 and D18. PK samples and samples for cytokine measurement were collected prior the start of the study on -D13 and 4h post-dose on D18. Hereto, whole blood was collected from the saphenous vein into serum separation tubes and stored at room temperature for at least 30 min. After 10 min centrifugation at ~2,000 x g, serum was collected and frozen at -80° C.

IG study with adjuvant:

Male BALB/c mice (BALB/cAnNCrI, from Charles River, age of 10 weeks, 5 animals per group) were dosed subcutaneously (2 x next to the inguinal region of the abdomen) once weekly 3 x on D1, D8 and D15 with 0.5 mg/kg of RTX WT + Allhydrogel® (Invivogen, #vac-*alu-250*) or vehicle control (PBS) + Allhydrogel®. Alum adsorption was done freshly on dosing day by 5 min incubation after 1:2 dilution of 0.05 mg/mL RTX in PBS in 10 mg/mL Allhydrogel. IG samples were collected prior to the start of the study on -D9 and pre-dose on D8 and D15. Spleen was collected after necropsy (sacrificed by CO₂ inhalation) on D16, weighted and placed into 50 mL vials containing 1 mL sterile medium L-15 + 10% FBS + 2 mM EDTA (Gibco, #15575020).

9.2. IG multiplex assay

Anti-RTX antibodies were measured using an ECL (electrochemiluminescence) based method on the MSD (Meso Scale Discovery®) platform. Using multispot plates coated with the four different RTX glycovariants (spot 8: WT, spot 1: N297A, spot 10: HiMan, spot 3: HySi) it was possible to measure potential glycovariant-specific mouse anti-RTX in one assay. Biotinylated RTX glycovariants were conjugated with spot-specific linkers (U-PLEX Linker Set 4-Assay 1 - 3 - 8 - 10, # N05229A-1) and coated (1 µg/mL) onto blocked (Blocking buffer: PBS + 0.05 % Tween 20 + 3 % BSA) MSD U-PLEX 4-Assay plates (#MESOK15229N-2). Plates were washed 3 x with PBS + 0.05 % Tween 20 and incubated for 1.5h at RT with mouse IG serum samples previously diluted 1:100 in Low cross buffer strong (LCB, Candor, # 102500). An anti-human IgG mouse IgG1 (R10Z8E9, produced in house) spiked into a mouse serum pool and diluted 1:100 in LCB strong was used as positive control at 0.1 and 10 µg/mL. Mouse serum pool diluted 1:100 dilution in LCB strong served as blank sample. Washed plates were incubated for 1h at RT with 0.02 µg/mL of a sulfo- or Ruthenium-tagged Fc-specific goat anti-mouse IgG (Sigma, #M4280) in LCB strong buffer. Finally, 2x Read buffer (MSD, # R92TC-3) was added to washed plates and incubated for 5 min before the plates were measured on the MSD S600 reader. The runs were accepted if the coefficient of variation (%CV) for the mean on duplicates was ≤ 30 % for positive controls, blank and IG samples. ECL signals were reported as anti-RTX IgG. A sample was considered as anti-RTX-positive if the ECL signal was above the threefold of the pre-dose median ECL signal across groups.

ECL signals from all 4 spots were comparable and shows that all RTX glycovariants were equally recognized by glycovariant-specific mouse anti-RTX confirming equivalent

sensitivity and specificity for all RTX glycovariants. Thus, ECL signals from only one spot, i.e. spot 8 coated with the WT, were reported.

9.3. PK assay

RTX mouse serum concentrations were measured using an ECL (electrochemiluminescence) based sequential bridging assay on the MSD (Meso Scale Discovery®) platform. The same goat anti-human IgG served as capture and detection antibody but was biotinylated (Southern Biotech, # 2049-08) as the capture reagent and sulfo-tagged (Southern Biotech, # 2049-01) as detection agent. For the assay, blocked (blocking buffer: PBS + 0.05 % Tween 20 + 3 % BSA) MSD Streptavidin plates (#L15SA-1) were coated with 1 µg/mL biotinylated goat anti-human IgG. Plates were washed 3 x with PBS + 0.05 % Tween 20. Post-dose mouse PK serum samples were diluted 1:20 in mouse serum pool while pre-dose samples not. Then, serum samples were diluted 1:100 in LCB strong, added to the coated, washed MSD plate and incubated for 1.5h at RT. RTX WT was spiked to a mouse serum pool at concentrations from 10 to 5000 ng/mL and diluted 1:100 in LCB strong to generate 8 standard samples. Blanks were generated by 1:100 dilution in LCB strong of mouse serum pool. Assay controls (quality control, QCs) included independently prepared RTX WT spike samples in the high (2000 ng/mL), medium (400 ng/mL) and low (50 ng/mL) range of the standard curve. Washed plates were incubated for 1h at RT with 0.2 µg/mL of the sulfo-tagged goat anti-human IgG in LCB strong buffer. Finally, 2x Read buffer (MSD, #R92TC-3) was added to washed plates and incubated for 5 min before the plates were measured on the MSD S600 reader. RTX serum concentrations were extrapolated from ECL signals using the fitted (4PL, weighting factor $1/Y^2$) standard curve. The runs were accepted if 6 of 8 standards were found within 80 – 120 % of the expected concentration, if all QCs were found within 75 – 125 % of the expected concentration and if the coefficient of variation (%CV) for the mean on duplicates was $\leq 25\%$.

9.4. Cytokine determination

Cytokine concentrations (CD40L, GM-CSF, IL-1, IL-4, IL-5, IL-6, IL-10, IL-12p70, IL-13, IL-15, IL-17A, IL17E/IL-25, IL-17F, IL-21, IL-22, IL-23, IL-27, IL-28B, IL-31, IL-33, MIP-3 α , IL-1 β , IFN γ , TNF α and TNF β) in mouse serum samples were measured using a 25-plex magnetic bead Milliplex MAP Kit (Millipore, #MT17MAG47K-PX25) on a Luminex MapPix instrument according to the manufacturer's protocol.

9.5. *Ex vivo* recall assay

Ex vivo recall was done with splenocytes isolated from animals immunized with RTX WT or with vehicle adsorbed in alum. Splenocytes from all animals collected at necropsy on D16 were isolated and processed into single cells and passed through a 40 μm strain. Erythrocytes were lysed for 5 min at 4°C in red blood cell lysing buffer (Sigma, #R7757). Isolated splenocytes were labeled with 0.5 μM CTVio (Thermo Scientific™, #C34557) at 37°C for 20 min. Free CTVio was captured by incubation with FBS for 5 min at RTX. After a final washing step CTVio+ splenocytes were seeded into 96 well plates (Costar, #3595) at 3×10^5 cells per well in X-Vivo (Lonza, #BE02-053Q) + 2 % Albumax (Gibco, #2117995) + 1 mM Hepes (Gibco, #15630-056) + 1 mM sodiumpyruvate (Gibco, #11360-070) + 1 x NEAA (Gibco, #11140-050) + 50 μM freshly added β -mercaptoethanol (Gibco, #31350-010). This serum-free medium has been determined as most optimal for stimulation of RTX-specific T cell responses from immunized mice in the *ex vivo* recall assay in preliminary experiments. Of note, no RTX-specific CD4⁺ T cell responses could be stimulated if done in medium containing FBS. *Ex vivo* recall was done with 1 and 10 $\mu\text{g}/\text{mL}$ RTX glycovariants, medium or 1 $\mu\text{g}/\text{mL}$ ConA (Sigma, #C5275) as positive control added on day 1 and day 4 (72 h). On day 6, cells were harvested and stained with surface marker antibodies for CD3 (Becton Dickinson, #553240), CD4 (ebioscience, #15-0041-83), CD25 (BD, #553072) and a viability dye (Lifetech, #L10119). CD4⁺ T proliferation and activation was measured on the Attune NxT flow cytometer.

10. Data analysis

All statistics and graphs were conducted in R Core Team (2020). R: A language and environment for statistical computing. R Foundation for Statistical Computing, Vienna, Austria. ISBN 3-900051-07-0, URL <http://www.R-project.org/>. Graphs were drawn using ggplot2 package. Statistical analysis was performed using statsr- and DescTools-, normality test using car-, multiple comparison statistical tests using ggpubr-, p-values added to graphs using ggsignif- and tables created with flextable-package.

Two group means were compared using the t-test if data were normally distributed (t.test()). Multiple comparison of means was done by One-way ANOVA Tukey's honest significant differences (Tukey HSD, aov(), TukeyHSD()) if data were normally distributed (shapiro.test() of residuals) and homoscedastic (equal variance, leveneTest()). If data were not normally distributed and heteroscedastic Kruskal Wallis chi-squared

(`kruskal.test()`) test was conducted to test whether group means are significantly different. A pairwise Wilcoxon signed rank test (`pairwise.wilcox.test()`) with Benjamin Hochberg correction (to control false discovery rate (24)) was subsequently conducted to test which groups are significantly different.

Results

1. RTX glycosylation modulates recognition by human DCs

Antibody Fc N-glycans are accessible to lectins. Fc-associated oligosaccharides were claimed to be buried in the Fc part of the antibody (11, 12). Therefore, it was speculated that these glycans may not be recognized by carbohydrate-specific binding proteins (lectins) (25). However, researchers use lectin microarrays to profile the glycosylation pattern of therapeutic antibodies such as evacizumab (Avastin®), trastuzumab (Herceptin®), adalimumab (Humira®), infliximab (Remicade®), and omalizumab (Xolair®), including rituximab (Rituxan®) which all bear solely Fc glycans (26), thereby invalidating the claim that Fc glycans are inaccessible.

In order to confirm Fc glycan accessibility for the in-house produced tool antibody rituximab, we conducted a Lectin ELISA. For this purpose, we selected lectins that could theoretically recognize RTX Fc glycans: AAL (*Aleuria aurantia* lectin) for recognition of the core α 1-6fucose (27), RCA-I (*Rhizinus communis* agglutinin) for non-reducing terminal Gal β 1–4GlcNAc (28), ConA (Concanavalin A) for the tri-mannose core Man α 1-6(Man α 1-3)Man (29) and DSA (*Datura stramonium* agglutinin) for GlcNAc β 1-4 (30) (Figure 1A). Binding of the glycosylated RTX (WT) to these biotinylated lectins was compared with that of the aglycosylated RTX (N297A) as a negative control (Figure 1B).

We observed binding to AAL, RCA and ConA because of the increased signal for the WT relative to the N297A. Further, we confirmed the specificity of the binding for RCA and ConA because respective soluble ligands suppressed the WT-derived signal (Figure 1C).

The data show that galactose and mannose structures present in the Fc glycan of RTX are accessible and may therefore be recognized by lectin receptors expressed by antigen presenting cells. We could not detect interaction with sialic acid because this carbohydrate is not present in the glycan of the WT.

Glycosylation facilitates binding and internalization by IDCs. To address the question whether RTX is recognized by DCs in a glycosylation-dependent manner, we assessed binding and internalization by immature dendritic cells (IDCs) using a FACS-based assay (assay principle see Supplementary Figure 2A). The difference in the binding signal at 4°C and the residual binding signal at 37°C were expressed as %internalization. We investigated glycosylation-dependency by comparing WT

(glycosylated) with the N297A (aglycosylated) variant. The WT (median internalization = 3.6 %) showed slightly increased internalization over the N297A (median internalization = 1.8 %) (Figure 2A). Although not being significantly different these data hint that glycosylation facilitates recognition by IDCs.

Mannosylation increases, sialylation decreases internalization by IDCs. Next, we wanted to know whether glycan modification on therapeutic antibodies affects the recognition and internalization by IDCs. Therefore, we changed the glycosylation of RTX to alter the interaction with activating or inhibitory lectin receptors by mannosylation and hypersialylation, respectively. Mannosylation of RTX increased the recognition and internalization (median internalization = 84.6 %) compared to the WT (median internalization = 3.6 %). Contrary, hypersialylation of RTX (median internalization = 0.2 %) decreased the recognition and internalization compared to the WT (Figure 2A). Altered glycosylation did not affect Fab-mediated binding to the target receptor CD20 because all RTX glycovariants showed equal binding to CD20⁺ Ramos cells (Figure 2B). Because of the high donor variability statistical analysis did not reveal significance. Nevertheless, the data hint that recognition by IDCs can be impacted by modifying RTX glycosylation.

Results from the FACS-based internalization assay indicate only residual RTX cell surface binding. In order to show that RTX is taken up into the cell, we assessed binding and internalization of fluorochrome-labelled RTX glycovariants by IDCs with confocal microscopy. Confocal images taken from IDCs incubated at 4°C show that RTX is solely localized at the cell surface characteristic of the expected ring structure of the fluorescence signal (Figure 2C). At 37°C RTX-derived fluorescence was detected in the cytoplasm adjacent to the nucleus (stained with DAPI) and not on the surface anymore (Figure 2D). The glycosylation-dependent binding and internalization pattern of RTX observed by FACS could be recapitulated: Aglycosylated RTX revealed lower binding and internalization relative to the WT, mannosylated RTX revealed strongest binding and internalization (Figure 2C, Figure 2D and Figure 2E). Interestingly the hypersialylated RTX showed a strong binding signal at 4°C comparable to that of mannosylated RTX. However, at 37°C we detected only very weak internalization for HySi. This observation suggests that the HySi is recognized by a different lectin receptor than the mannosylated RTX. This unknown receptor seems to cause a strong interaction but does not result in internalization of bound ligands and may therefore exert an inhibitory function.

Mannosylation increases, sialylation decreases routing of RTX into degradative endolysosomal pathway. Next, we assessed the effect of RTX glycosylation on the endosomal routing. For this, we stained IDCs with the lysosomal marker Lamp-1 after internalization of fluorochrome-labelled RTX. RTX was detected in lysosomal compartments and this effect was strongly associated with the glycosylation-pattern (Figure 3A). Consistent with the strongest internalization of mannosylated RTX, this glycovariant caused most prominent routing into the lysosome. In contrast, hypersialylated RTX demonstrated weak or no detectable co-localization with the lysosome. The N297A showed similar or slightly lower co-localization with Lamp-1 relative to WT. In addition to Lamp-1, we used EEA1 and Rab7 as markers to assess potential glycosylation-related differences in the routing into the early and late endosome, respectively. We detected strong co-localization with both markers for HiMan, moderate co-localization for WT, weak co-localization for N297A and almost no detectable co-localization for HySi (Figure 3B and Figure 3C). At the tested time point (2 h) co-localization of HiMan and WT with the late endosome seemed to prevail. For N297A and HySi we could not observe a difference in routing into either the early or late endosome likely because of the low internalization. In summary, the data show that RTX glycosylation determines the pattern of intracellular uptake by IDCs. In addition, we show that mannosylation increases and hypersialylation decreases routing of RTX into the degradative pathway.

IncuCyte internalization assay confirms effect of mannose and sialic acid on glycosylation-dependent uptake of RTX by IDCs. The FACS-based internalization assay does not allow an easy capture of the internalization over time. In addition, internalization can only be determined indirectly from the loss of surface-bound RTX at 37°C. Therefore, we established an alternative method based on real-time imaging with the IncuCyte analyzer. Using this new assay, we achieved better kinetic measurements (Supplementary Figure 2B) and were able to quantify internalization from an increase of the fluorescence signals within the cell using fluorochrome-labelled antigens. Measuring the glycosylation-specific internalization of RTX by IDCs with the IncuCyte assay confirmed that mannosylation increased and hypersialylation decreased internalization (Figure 4A and Supplementary Figure 2B) at all measured time points. More specifically, mannosylated RTX exerted ~5x higher internalization relative to the WT while HySi exerted only half of WT internalization. Different to previous results the N297A showed in

median a slightly higher internalization than the WT. Nevertheless, some donors presented the previous pattern with an increased internalization of the WT over N297A (Supplementary Figure 2C).

We compared the slopes of the fluorescence signals over time obtained from each glycovariant. The slope is a measure to indicate the internalization rate per time unit. HiMan exerted the highest slope (0.272), followed by WT (0.016) and N297A (0.0156). HySi revealed the lowest slope (0.012). Thus, HiMan shows the highest while HySi the lowest internalization rate/speed.

2. RTX glycosylation modulates recognition by human T cells

Mannosylation increases T cell activation in humans. Next, we wanted to know whether glycosylation-mediated effects on internalization observed for RTX influence T cell activation. Therefore, we investigated internalization along with T cell activation in the same donor set (treatment-naive donors). We stimulated T cells at 10 $\mu\text{g/mL}$ of each RTX glycovariant, the same concentration as applied for the internalization assay. Absolute counts of proliferating and activated Th cells were determined at priming and challenging and expressed as stimulation index (SI, Figure 4C) indicating the challenge response relative to the priming response induced by each RTX glycovariant. Donors showing an SI above 1.5 were assigned as T cell responders and used to determine the percentage of responding donors expressed as response index (Figure 4D). Five of 16 (31 %) donors showed a WT-specific response (Figure 4C and Figure 4D). Mannosylated RTX mounted an increased T cell response compared to WT with 8 responders of 16 tested donors (50 %, Figure 4D). Hypersialylated RTX mounted a slightly decreased T cell response compared to WT with 4 responders of 15 tested donors (26.7 %, Figure 4D). Of note, counts of proliferating CD25⁺ Th cells were remarkably lower if T cells were primed and challenged with HySi compared to all other RTX glycovariants (Figure 4B). Unexpectedly, aglycosylated RTX demonstrated similar or slightly higher T cell activation (7 of 13 donors) compared to mannosylated RTX (54 %, Figure 4D). Donors were dissected in WT responder and WT non-responder (Figure 4C). None of the WT responder was reactive to hypersialylated RTX, while few WT responders were reactive to HiMan and N297A. The positive control tetanus toxoid (TT) induced strong T cell activation (determined as CD25 upregulation) and proliferation while the medium control did not, indicating a good assay performance (Supplementary Figure 3A and 3B).

In summary, these data hint that T cell responses can be enhanced or dampened if the glycosylation pattern is modified. While mannosylation enhances T cell responses compared to WT, hypersialylated RTX is not recognized by WT responder T cells and suggests that sialylation of RTX does either cause less efficient antigen presentation, does not provide co-stimulatory signals to activate pre-existing WT-reactive T cells or/and promotes polarization to Tregs.

To determine whether internalization and T cell activation are dependent on each other, both measures obtained from the same donor were correlated (Figure 4E). Apart from the aglycosylated RTX, glycosylation-dependent T cell responses were concordant with glycosylation-dependent internalization. However, an association of internalization with T cell activation could only be observed for the HiMan ($r = 0.34$) but not for the WT ($r = 0.015$) (Figure 4E).

In summary, these data suggest that increased DC internalization caused by mannosylation of RTX can lead to increased recognition and activation by T cells. For other glycosylation patterns or lacking glycosylation, T cell response did not seem to depend on internalization.

Glycosylation co-determines T cell recognition in humans. To assess whether RTX glycovariants share T cell determinants, we measured T cell responses induced by the glycovariants relative to the prime response induced by the WT (Figure 5A and Figure 5B). Three of 10 naive human donors showed a WT-specific response. Donors were dissected in WT responder and non-WT responders (Figure 5C). The mannosylated RTX was able to re-stimulate T cells primed with the WT (2 of 10 donors, 20 %) while hypersialylated RTX or aglycosylated RTX was not. The lacking T cell reactivity for HySi and N297A to the WT suggests that HySi and N297A possess T cell determinants different from the WT. Since some WT responders were reactive to HiMan, this glycovariant seems to share determinants with the WT. Non-WT responders could not be re-stimulated with any of the glycovariant and confirms that the detected T cell responses are specific to the WT. Taken together, these data imply that glycosylation may co-determine T cell recognition.

3. Lectin receptors and FcγRs mediate recognition of RTX by human DCs

Lectin receptor and FcγR expression. Uptake of extracellular components into the cell can occur through receptor-independent or receptor-dependent mechanisms (31). For the latter, lectin receptors, specialized to recognize carbohydrate structures on pathogens but also on self-proteins (32), are known to internalize glycosylated antigens (33). FcγRs facilitate uptake of bound IgG via the Fc region (34). This FcγR - Fc interaction is largely affected by Fc-glycosylation (35). Therefore, these receptors may drive or contribute to the glycosylation-dependent internalization observed for RTX. Expression of selected lectin receptors (DCIR, DC-SIGN, CD206, DEC-205, Siglec 7) and the three main FcγRs (FcγRI = CD64, FcγRII = CD32 and FcγRIII = CD16) was determined along with internalization of RTX glycovariants on IDCs from the same donor set (Supplementary Figure 4A and 4B). Lectin and FcγR expression were highly variable except for CD64, DEC-205 and DC-SIGN. CD64 and DEC-205 expression was low (median % frequency: 1 % and 0.18 %, respectively), DC-SIGN expression was high (median % frequency: 95.4 %) as reported in the literature (36, 37). Similarly, glycosylation-dependent internalization varied (Supplementary Figure 4B). The relationship between glycosylation-dependent internalization and lectin/FcγR expression on IDCs was assessed (Supplementary Figure 4C). Overall, association between internalization and LR/FcγR expression was moderate. Nevertheless, correlation coefficients were higher if RTX carried glycans (WT, HiMan or HySi) and lower if RTX lacked glycans (N297A), as shown for correlations between internalization and expression of CD32, CD64, CD206, DC-SIGN and Siglec 7.

Altogether, the data suggest that the endocytosis mechanism is determined by presence or absence of glycosylation meaning that aglycosylated RTX may be internalized in a receptor-independent manner while glycosylated RTX may be internalized in a receptor-dependent manner.

Effect of LR blockade on glycosylation-dependent uptake by IDCs. To prove that lectin and/or FcγR receptors mediate internalization of RTX glycovariants, we assessed internalization in presence of receptor ligands or recombinant proteins as blocking agents. Pre-incubation with full length IgG completely abrogated internalization of WT and HiMan (Figure 6A). Full blockade is expected because full length IgG provide Fc N-glycan structures that can compete with glycosylated RTX for FcγRs and lectin receptors. To assess the role of CD32 for internalization, the main FcγR expressed by IDCs (35), we

used a CD32-targeting F(ab)², which facilitates blockade in a glycosylation-independent manner because of the lacking Fc and its glycan. A role of CD32 in internalization of WT and HiMan could be demonstrated because internalization was attenuated with increasing concentration (Figure 6B). Because CD32-blockade only partially blocked internalization, other receptors such as lectin receptors may drive receptor-dependent internalization. Indeed, if IDCs were pre-incubated with Mannan, a multivalent ligand of Mannose-binding lectins receptors (38), blockade of internalization was most prominent for mannosylated RTX and least prominent for aglycosylated RTX (Figure 6C).

Next, we pre-incubated IDCs with recombinant lectin receptors. Recombinant human DC-SIGN or CD206 did not exhibit any effect on internalization (Figure 6D). Therefore, it could not be demonstrated that mannosylated RTX is recognized by these receptors, albeit mannosylated glycan structures were ascribed to recognition and internalization by IDCs. Siglec 7, as potential lectin receptor to recognize Neu5Ac α 2-6Gal β 1-4GlcNAc containing sialoglycans (39, 40), was blocked by pre-incubation with its recombinant human protein. Indeed, internalization of HySi was attenuated in presence of recombinant huSiglec 7 (Figure 6E). Internalization of WT was also slightly decreased by Siglec 7 blockade, albeit weaker than that of HySi. This inhibition cannot be attributed to sialoglycans because the WT does not contain such glycans.

In summary, these data show that internalization of glycosylated RTX is partially driven by CD32. Recognition of mannosylated RTX is glycosylation-specific. Siglec 7 seems to be important for recognition of hypersialylated RTX.

4. RTX glycosylation modulates the immune response and clearance in mice

Mannosylation increases the humoral immune response in BALB/c mice. Utilizing aforementioned *in vitro* approach, we were able to assess the influence of RTX glycosylation on the uptake, routing and presentation by antigen presenting cells and on the recognition by T cells, i.e. on human T cell immunogenicity. To understand whether changes in glycosylation affect B cell responses, we conducted *in vivo* experiments in BALB/c mice. In a preliminary study BALB/c and C57BL/6 mice were compared to identify a suitable strain that mounts a robust antibody response to RTX. BALB/c mice were shown to be more sensitive to immunization with RTX than C57BL/6 mice (Supplementary Figure 5A). Therefore, this strain has been chosen to assess glycosylation-dependent immunogenicity to RTX.

Anti-RTX antibodies (IgG isotype) were determined at baseline (D-13) and before each dose (except before the 1st dose on D1). Until D4 (after the 2nd dose), none of the animals had detectable ADAs (Figure 7A). On D8 (3rd dose), ADAs were detected in 2 of 10 animals dosed with the WT, but not in animals dosed with other RTX glycovariants. On D15 (5th dose), the majority of animals (6/10) dosed with the WT mounted a response. On D18 (6th dose), this response slightly dropped (4/10). Compared to the WT, HiMan induced a higher ADA response on D18 (Figure 7A). In contrast, the N297A induced a weaker ADA response on D11, D15 and D18 (Figure 7A) compared to the WT. The ADA profile of HySi was comparable to the WT (Figure 7A).

These data show, that changes in RTX glycosylation impact the humoral response i.e. ADA formation. Importantly as observed *in vitro* using human DCs, mannosylation of RTX increased the immune response to RTX in BALB/c mice. Contrary to human *in vitro* results, lack of RTX glycosylation decreased while hypersialylation of RTX did not change the immune response to RTX in BALB/c mice.

Mannosylation increases T cell activation in an ex vivo recall assay. The next question was whether we can recapitulate the glycosylation- and Th-cell-dependent humoral response in mice. Therefore, BALB/c mice were immunized with 3 doses of WT in conjunction with the adjuvant alum. In the previous study, conducted to measure immunogenicity in response to RTX glycovariants, it was not possible to detect a RTX-specific T cell recall response. Therefore, the adjuvant alum was used in this study to maximize the immune response to RTX. ADAs were measured to demonstrate that this new immunization protocol worked. Four of 5 animals had detectable ADAs on D15 after 3 injections of WT. No animal had ADAs at any time point in the control group (Supplementary Figure 5B). The response to the WT could be increased from 60 % as observed in the previous study to 80 % by the use of the adjuvant alum (Supplementary Figure 5C) with 3 instead of 6 injections.

To assess glycosylation-dependent T cell responses, we isolated immune cells from spleens of WT and control (adjuvant only) animals and performed an *ex vivo* recall assay. Absolute counts of proliferating and activated Th cells after stimulation with the RTX-glycovariants were determined relative to the medium control after two *ex vivo* challenges and expressed as stimulation index. The positive control ConA induced strong activation and proliferation of Th cells in 4 of 5 animals in the control (median SI = 11.4,

Supplementary Figure 5D) and the treatment group (median SI = 31.7, Figure 7B). The WT demonstrated a T cell response in 3 of 4 animals above the SI threshold of 1.5 (median SI = 2.4). The response was specific to RTX because no T cell response could be recalled in control animals immunized with adjuvant only (Supplementary Figure 5D). The HiMan group showed a slightly higher (median SI = 2.6) and the N297A cohort a lower (median SI = 1.7) T cell response compared to the WT. The response to the HySi was between that observed for WT and N297A (median SI = 2.0). The T cell recall responses induced by RTX glycovariants were not significantly different likely because of the small group size. Nevertheless, the results from the *ex vivo* recall assay recapitulate the humoral glycosylation-dependent response pattern (HiMan > WT ~ HySi > N297A). In addition, these data indicate that humoral responses are T cell dependent.

Mannosylation increases RTX clearance in BALB/c mice. In order to demonstrate that all animals in the treatment groups were exposed to RTX, we determined serum concentrations of RTX at baseline (-D13) and 4h post-dose on D1 and D18. As expected, RTX could be detected post-dose in serum of all animals in RTX glycovariant treatment groups and not in the control group animals (Figure 7C).

Furthermore, we aimed to assess the effect of RTX glycosylation on the clearance of RTX. Such association of clearance with glycosylation has been described in the literature (6, 41-43). On average, RTX levels were remarkably higher after 6 doses (D18) than after one dose (D1) but not in all animals and not for the HiMan group (Figure 7C). The reduced exposure on D18 relative to D1 observed in a fraction of animals and in the HiMan group may be explained by the presence of anti-drug antibodies. Therefore, we assessed the relationship between immunogenicity (anti-RTX antibodies) and RTX exposure (Figure 7D). Animals with high immunogenicity presented low exposure ($r = -0.81$). This negative association is well known and caused by clearance of protein-ADA immune complexes by the reticuloendothelial system (44-46) or by the inability to detect RTX complexed by ADAs in the pharmacokinetic (PK) assay. This means that the significantly reduced exposure observed for HiMan relative to WT on D18 (Figure 7D) is attributed to ADAs and not to direct effects of glycosylation on the clearance. For this reason, it is only possible to assess glycosylation-related effects on clearance on D1, when no ADAs have formed yet. Interestingly on D1, we only observed a significantly decreased exposure for the HySi (median exposure = 396 ng/mL) while the exposure of N297A (median exposure

= 676 ng/mL) or of HiMan was not significantly changed, albeit that of HiMan (median exposure = 582 ng/mL) was slightly lower relative to WT (median exposure = 701 ng/mL).

Taken together, these data hint that glycosylation impacts the clearance of RTX in BALB/c mice. Hypersialylation and mannosylation of RTX appear to increase the clearance. The effect of hypersialylation on the clearance seems to be transient because it was not detected at the end of the study anymore. If glycosylation is absent the clearance was not affected.

RTX glycovariants evoke specific cytokine response pattern. Specific immune pathways – including those involved in T cell differentiation – are influenced and characterized by specific cytokine profiles. Therefore, we measured various cytokines covering $T_H1/T_H2/T_H17/T_H21$ differentiation pathways in the serum of mice immunized with the different RTX glycovariants pre-dose, on D1 and D18 4h post dose.

A specific cytokine pattern was observed for animals immunized with different RTX glycovariants (Figure 8). Significantly increased levels relative to pre-dose were detected in animals immunized with HiMan for IL-28B on D1 and for $TNF\alpha$, IL-6 and IL-21 on D18; for $IFN\gamma$, IL-17A and IL-4 on D1 and D18 immunized with the WT; for IL-5 (D1 & D18) and IL-22 (D18) immunized with HySi. In addition, the regulatory T cell cytokine IL-10 was significantly elevated on D18 as the only cytokine that was stimulated by the aglycosylated RTX but also by WT and HySi while not by HiMan. No changes were detected for IL-2, GM-CSF, MIP-3 α , IL-1 β , IL-27, IL-23, IL-12p70, IL-13, IL-15, IL-17A, IL-17F, IL-31, IL-33, $TNF\beta$ and CD40L.

These data suggest that each glycovariant induced a specific cytokine response pattern supporting a distinct T cell polarization. HiMan stimulated a T_{FH}/T_H1 (T follicular helper) response (as detected by high IL-21, high IL-6 and low $TNF\alpha$). HySi induced a T_H2 dominant response (indicated by high IL-5, low IL-22 and low IL-10). WT induced an assortment of $T_H1/T_H2/T_H17$ responses (indicated by high $IFN\gamma$, high IL-4, high IL-17A and low IL-10). Contrary, N297A caused a response solely characteristic of IL-10 without any other significant cytokine involvement, indicating an immunoregulatory response.

Discussion

Glycosylation-dependent recognition by DCs

This work provides new insights concerning the role of antibody glycosylation for antigen recognition and immunogenicity. First, we demonstrate that the Fc glycans of the tool antibody RTX are accessible for recognition by the plant lectins ConA and RCA and may therefore be recognized by lectin receptors expressed by DCs. Indeed, we show here that the Fc glycan is important for recognition by DCs because the glycosylated RTX clearly binds to DCs, unlike the aglycosylated RTX (Figure 2C), which is only internalized to a low extent (Figure 2D). Thus, we conclude that uptake is mediated in a receptor-independent manner i.e. by constitutive macropinocytosis (“cell drinking”). Because macropinocytosis is a less efficient DC uptake mechanism it explains why less RTX is internalized by DCs if glycans are missing. In contrast if RTX is glycosylated, DC uptake seems to be dominated by the more efficient process of receptor-mediated endocytosis as facilitated by LRs.

Secondly, in the present work we further show for the first time that antibody Fc mannosylation increases DC uptake and routing into the degradative endo-lysosomal pathway compared to an antibody with a complex-type glycosylation (Figure 2A, Figure 2C, Figure 2D). The specificity of the effect of mannosylation on DC uptake was proven by the ability to inhibit DC uptake in presence of mannan (Figure 6C).

Furthermore, we show that extension of the complex type Fc glycan by sialic acids (i.e. hypersialylation) decreases DC uptake and routing into the degradative endo-lysosomal pathway (Figure 2 and Figure 3). Fc glycans of RTX were extended in α 2-6 linkage with sialic acids. Because RTX HySi variant was not available in α 2-3 linkage it cannot be concluded whether α 2-6 linkage is indispensable to decrease DC recognition and uptake of RTX.

Contrary to our results, sialylation of antibody Fc did not reduce antigen uptake by DCs nor DC maturation (47). This discrepancy may be explained by the fact that their study was done with glyco-modified adalimumab. Since TNF α , the target of adalimumab, is expressed by DCs in its transmembrane form the dominating DC uptake mechanism

seems to be target-mediated. Thus, weak glycosylation-mediated effects may be masked under these conditions.

In addition, this work shows that glycosylation-dependent recognition of RTX is facilitated by DC-associated receptors. LRs and FcγRs are potential candidate receptors because they recognize carbohydrates or binding highly depends on the presence and composition of Fc glycans, respectively. Aglycosylated antibodies lack and specific Fc glycosylation (galactosylation, mannosylation, sialylation, fucosylation) modifications alter FcγR binding. Hence it is possible that the observed difference between the glycosylated and aglycosylated RTX is ascribable to FcγR binding. Not only FcγRs mediate the binding of RTX because binding and internalization was only partially suppressed upon CD32-blockade. CD32 or FcγRII is the main FcγR receptor expressed by IDCs. As FcγRI and FcγRIII IDC-expression is negligibly low, these receptors are not considered as relevant for uptake of RTX. In contrast, the expression of LRs such as DC-SIGN, MR, DCIR and Siglec 7 by IDCs was abundant (Supplementary Figure 4A). Thus, it is possible that these carbohydrate specific LRs are involved in the recognition of Fc glycans. Some of the glycan recognition motifs reported for LRs (such as terminal GlcNAc, high mannose, terminal galactose, sialic acid) are present on Fc glycans, hence may be recognized by LRs. The majority of the CLRs (e.g. DC-SIGN, MR, DCIR) carry the EPN/EPS motif which allows binding of mannose, GlcNAc, fucose and glucose. The QPD motif attributes to recognition of galactose or GalNAc and is present in DC-ASGPR (Dendritic cell asialoglycoprotein receptor) and MGL (Macrophage galactose N-acetylgalactosamine specific lectin) (48-50). Nevertheless, each CLR has unique binding preferences and affinities to glycans. Since DCs express multiple CLRs it is likely that the receptor which yields the highest affinity/avidity will dominate recognition of Fc glycans.

Because FcγRII expression on DCs does not correlate with DC uptake of any glycovariant FcγRII does not appear to drive the recognition. Therefore, we conclude that LRs are more likely to account for it. This assumption is supported because LR expression with ligand specificity for sialic acid and oligo-mannose correlates with glycosylation-specific DC uptake (Supplementary Figure 4C). More specifically, Siglec 7 expression on DCs correlates with DC uptake of HySi while DC-SIGN and MR expression with that of HiMan. The lacking correlation of LR expression and internalization of the aglycosylated RTX confirms that DC uptake is receptor-mediated and glycosylation-dependent. Expression

of MGL, DC-ASPGR were not monitored on IDCs because these receptors are not reported to recognize high mannose and sialoglycans although galactosylated species present in WT Fc glycans may serve as ligands. Inhibition experiments were focused on deciphering the role of DC-SIGN, MR and Siglec 7 because the expression of these receptors correlated with the uptake of RTX glycovariants.

We demonstrated that HySi internalization is partially mediated by Siglec 7. Siglec 7 inhibition downregulated DC uptake of HySi, while not of HiMan and N297A (Figure 6A). It is possible that other Siglecs than Siglec 7 known to recognize terminal Neu5Ac α 2-6Gal β 1-4GlcNAc (i.e. Siglec 9 and 10) and/or other LRs are involved in the DC recognition of HySi. Sialylation of Fc glycans decreases its capacity to interact with type I Fc γ R_s while that with the type II Fc γ R DC-SIGN is supposed to increase (51). This increased engagement of DC-SIGN by sialylated IgG was shown to upregulate Fc γ R1b expression by IL-33 and IL-4 release in mice (52) and was proposed as mode of action for the anti-inflammatory effects of high dose MIG. If HySi RTX could trigger a similar effect in human DCs an upregulation of Fc γ R1b could increase the threshold for activation of receptors potentially targeted by HySi. However, other literature does not support that DC-SIGN is targeted by sialylated IgG (53) or that anti-inflammatory effects of MIG are attributable to Fc-associated sialoglycans (54). Finally, there is no apparent evidence that the CRD of DC-SIGN directly recognizes sialylated glycans. For these reasons, DC-SIGN was not considered as relevant LR for recognition of HySi.

We could not show that MR or DC-SIGN drive the recognition of HiMan by inhibition experiments. In theory, the HiMan oligo-mannose should fulfill the structural prerequisites to be recognized by MR. For DC-SIGN, it seems that N-linked oligo-mannose glycans cannot be recognized (55) and may explain why internalization of HiMan could not be blocked in presence of recombinant human DC-SIGN. In order to provide clear evidence that MR and/or DC-SIGN do or do not recognize HiMan binding experiments using cell lines transfected with DC-SIGN or MR would be required. Nevertheless, it appears that mannosylation destines the routing of RTX because it was preferentially detected in the late endosome and lysosome at the measured time point RTX as reported by others (56, 57), thus enhances the uptake and routing for proteolysis.

Glycosylation-dependent T cell recognition

Furthermore, we show that RTX glycosylation affects antigen presentation and T cell recognition. Mannosylation of RTX increases and sialylation of RTX decreases T cell responses (Figure 4D). Thus, glycosylation-specific DC uptake correlates with antigen presentation (Figure 4E). Consistent with these findings, enhanced T cell responses have been previously observed for mannosylated OVA which were driven by CLR-mediated uptake and subsequent routing into the degradative pathway (55).

That sialylation can induce antigen-specific tolerance has been previously shown in mice using sialylated OVA and MOG₃₅₋₅₅ (58). In that study it was found that Siglec E, the murine orthologue of human Siglec 7/9, is required to stimulate tolerogenic DCs and regulatory T cells and therefore inhibits effector T cell responses. This is in line with the observed reduced human T cell response for hypersialylated RTX relative to the unmodified RTX in our study. Additional experiments (e.g. showing whether HySi RTX induces FoxP3⁺ Tregs and whether immunosuppressive cytokines are secreted by DCs) may further substantiate this likely relationship.

Interestingly, aglycosylated RTX stimulated T cell responses in a similar manner as mannosylated RTX, although DC uptake of the aglycosylated RTX was much lower compared to the mannosylated RTX (Figure 4A). This observation might suggest that aglycosylated RTX is more easily processed by endolysosomal proteases which increases peptide generation and presentation on MHCII. Glycosylation of amino acids near the proteolytic cleavage site can block proteolysis and therefore prevent peptide cleavage for MHC presentation which has been shown previously for MUC1, a heavily glycosylated tumor antigen (59) but also for viral glycoproteins (60, 61). One needs to consider that aglycosylated RTX possesses a single point mutation i.e. N297A. It is unlikely that this minor deviation in the Fc peptide sequence from the other RTX glycovariants accounts for the enhanced antigen presentation but it cannot be formally excluded.

In vitro assays have the advantage that immuno-regulatory mechanisms can be assessed using human immune cells which may be more relevant for studying clinical immunogenicity than studies in mice. Based on interaction and restriction to specific human MHCII alleles, potential immunogenic epitopes can be identified and removed if not required for the activity. Such epitope mapping is done using antigen-specific T cell lines or clones which are screened for reactivity to peptides bearing potentially

immunogenic amino acid sequences. In a similar approach, reactivity of enriched RTX-specific T cells was tested for glycosylation-dependency/specificity (Figure 5). The aglycosylated and hypersialylated RTX were not able to re-stimulate WT-specific CD4⁺ T cells. Therefore, it is plausible to conclude that the glycosylation pattern determines the peptide presentation by MHCII and therefore influences the recognition by CD4⁺ T cells. Interestingly, mannosylated RTX was able to re-stimulate WT-specific CD4⁺ T cells in a few but not all donors. Hence, HiMan seems to share CD4⁺ T cell determinants with WT RTX. These experiments were neither done with highly enriched RTX-specific CD4⁺ T cells nor with clones. In addition, *in vitro* assays were performed with immune cells from treatment-naive subjects. Thus, CD4⁺ T cell responses stimulated under these conditions are much weaker compared to those from treated patients. Therefore, CD4⁺ T cell responses could only be detected in few donors that may react to RTX because of pre-existing CD4⁺ T cells that arose from previous exposure to an antigen highly homologous to structures of RTX. For these reasons, it would be beneficial to study glycosylation-dependent and -specific effects on T cell immunogenicity using T cell lines or clones generated from RTX-treated patients that formed ADAs.

Rituximab CD4⁺ T cell epitopes have been described in the variable region using PBMCs from healthy human subjects (62). Based on these data it may be counterintuitive to suggest that a modification present in the Fc region could affect epitopes in the variable region. Epitope spreading, i.e. a shift from recognition of immuno-dominant to subdominant epitopes, can result from altered uptake and processing (63). Cryptic T cell epitopes (i.e. determinants that are usually not formed but could be recognized by a specific TCR) may become dominant because of altered glycosylation or deglycosylation. Since T cell epitopes for RTX WT and glycovariants were not determined, it cannot be concluded that glycosylation causes epitope spreading. However, because it was demonstrated that RTX glycosylation influences DC uptake and recognition by T cells it may be an explanation. In order to determine the exact T cell epitope, glycopeptides or peptides could be eluted from MHCII and determined by MS proteomics analysis. If glycopeptides were presented by MHCII these could be tested for their ability to stimulate RTX-specific CD4⁺ T cells and glycopeptide-specific CD4⁺ T cell clones generated and used to further characterize the specificity of the TCRs against the glycan, the peptide or the glycopeptide (64, 65). Further, to confirm glycosylation- and LR-dependency one

would need to demonstrate that CD4⁺T cell responses can be suppressed in presence of glycans (such as mannan) or LR-blocking proteins.

Glycosylation-dependent humoral immune response

Having demonstrated that T cell immunogenicity is affected by antibody glycosylation we sought to study its impact on the humoral immune response. Because we show that mannosylation of RTX increases B cell immunogenicity (Figure 7A) we demonstrate here to our knowledge for the first time that antibody glycosylation also influences humoral immune responses. These results are in agreement with the antigen-uptake, processing and presentation results obtained in human *in vitro* assays for mannosylated RTX. However, the apparent tolerogenic effect of sialylation and immunogenic effect of aglycosylation found in human *in vitro* studies could not be recapitulated in the mouse study. Instead aglycosylated RTX was least immunogenic in mice suggesting, as initially postulated, that antibody glycosylation facilitates recognition and immune responses. This result is in line with previous studies, for example on the tumor antigen Muc1 or on the rheumatoid arthritis autoantigen collagen type II (CII) where humoral responses fail if glycosylation is absent indicating that the immunogenic epitopes are determined by the glycoprotein (66-69).

We could not show that HySi induces tolerance in mice as observed in human. Murine Siglecs may not be recognized by α 2-6-linked sialoglycans as present in HySi, thus explaining the discrepancy. Nevertheless, the TH2 dominant cytokine pattern (high IL-5, low IL-22) induced by HySi was different from the inflammatory TH1/TH2/TH17 profile of the WT (high IFN γ , high IL-4, high IL-17A) (Figure 8), and thus implies that HySi engages other receptors with signaling capacity than the WT. Despite these differences the ADA responses for HySi and WT were comparable.

Humoral and cellular responses in the mice were concordant i.e. *ex vivo* recall performed with aglycosylated RTX induced weak CD4⁺ T cell responses relative to the WT while mannosylated RTX induced strong CD4⁺ T cell responses (Figure 7B). Thus, glycosylation-dependent CD4⁺ T cell recognition seems to differ in mouse and human. The results obtained in mice may not be predictive for humans. Since glycosylation-dependent effects on T cell responses were translatable to glycosylation-dependent humoral immune responses in mice it is plausible that low T cell immunogenicity as

observed for hypersialylated RTX observed in human translates to low anti-drug antibody response in human, but this remains to be shown.

Glycosylation-specific anti-RTX responses were also reflected in glycosylation-specific serum cytokine patterns (Figure 8). IL-21, characteristic of a T_{FH} response known to promote germinal center reactions and memory B cell responses, was only detected for HiMan. This finding is in line with the highest immunogenicity induced by HiMan. Another cytokine that was uniquely secreted by HiMan was IL-28B. IL-28B is induced in response to viral infections (70). Since viruses carry mannosylated glycans, as HiMan does, there seems to be an association between the recognition of mannosylated glycans and the secretion of IL-28B. IL-10, characteristic of a regulatory response, was the only cytokine elevated after N297A immunization and is in agreement with the lowest IG induced by this aglycosylated RTX. It is likely that this glycosylation-specific T cell polarization results from the ability of each glycovariant to interact with a unique LR or set of LRs. Differential or cooperative signaling cascades induced by DC-associated LRs may shape the T cell response and in turn the humoral B cell response. Upon immunization with RTX some of the cytokines were elevated only on D18 4h post-dose and not yet on D1 4h post dose. This observation supports the notion that T cell polarization is not only regulated by binding of monomeric RTX to LRs but also by binding of RTX-ADA immune complexes to FcγRs. Since the aglycosylated RTX does not bind to FcγRIIs the abovementioned proposed mechanism may be less relevant to aglycosylated RTX in line with its lacking inflammatory cytokine response.

FcγRs can be triggered not only by IgG but also by IgE in mice. Such an IgE ligation skews T_{H1} to T_{reg} cell responses by suppressing the secretion of IL-12 and increasing IL-10 by DCs (Blink and Fu 2010). Mice immunized with N297A showed only low IgG anti-RTX levels (Figure 8A) and an exclusive IL-10 secretion (Figure 8). It would be interesting to know whether this N297A-specific IL-10 signature is associated with a favored IgE isotype-switch induced by the aglycosylated RTX. However, such a mechanism would not be relevant in human because IgE does not bind to FcγRs in man (72). These and other species-specific differences in the FcγR expression, distribution, function and ligands (73-75) could be a reason for the discrepancy between mouse and human results on N297A and HySi immunogenicity.

Glycosylation-dependent clearance

We also demonstrate here that antibody glycosylation impacts clearance. RTX exposure was slightly reduced if mannosylated (Figure 7C) which is concordant with previous reports (76-79) although others do not report effects of high mannose glycans on antibody clearance (25, 80). For therapeutic proteins Epo, FVIII, β -glucocerebrosidase clear effects of glycosylation on clearance were reported. These effects were attributed to binding to ASGPR and MR expressed in the liver by hepatocytes or Kupffer cells, respectively. Deglycosylation of FVIII decreases the clearance (81). Desialylation of β -glucocerebrosidase and pegylated Epo markedly increases the clearance (82, 83). Thus, it is expected that sialylation has the opposite effect i.e. decreases the clearance by masking terminal galactose residues (84). In line with this, Bas et al. (85) ascribe the observed increased half-life of antibodies, mutated in the Fc to increase FcRn ligation, to sialic acids independent of FcRn, Fc γ R1Is and structural effects. Indeed, a role of ASGPR for the increased clearance of afucosylated and fucosylated pertuzumab by desialylation could be proven (42). However, earlier studies were not able to demonstrate such an effect of sialylation on clearance. Kaneko et al. (4) did not observe that sialylated MIG (lectin fractionated) was cleared slower or faster compared to non-fractionated MIG. Another study using desialylated anti-TNF α could also not report a different PK profile compared to the sialylated antibody (86) and mono- and di-sialylated antibody Fab glycans did not affect the PK profile (25).

In the current study, hypersialylated RTX showed slightly decreased exposure (Figure 7C). There is one report which claims that ASGPR recognizes α 2-6 linked sialoglycans (Sia α 2-6Gal β 1-4-GlcNAc) and not α 2-3 linked ones thus may promote the clearance of endogenous glycoproteins (87). In addition, they hypothesize that terminal β 1-4Gal linked glycans are cleared independent of ASGPR. Another study confirms that the linkage is relevant because a glycoprotein containing α 2-6 linked sialoglycans was cleared faster than that containing α 2-3 linked sialoglycans (20), thus exhibited a lower activity. Therefore, it may be possible that the reduced exposure of HySi detected in BALB/c mice accounts to a preferred recognition of α 2-6 linked sialic acids by ASGPR.

One must consider that the main purpose of the *in vivo* study in BALB/c mice was to assess glycosylation-dependent immunogenicity. RTX concentrations were primarily determined in order to confirm exposure in all treated animals. Therefore, only a limited number of samples was collected to measure RTX concentration. To get a better

Accepted Article

understanding on glycosylation-dependent exposure one would need to sample frequently after a single dose (2h, 6h, 24h, D1, D2, D4, D6, D12) to calculate different PK parameters (e.g., half-life, AUC, distribution volume at steady state, mean retention time and clearance).

The contradictory results for the role of antibody-sialylation on biological effects such as on the clearance may be based on the heterogeneity of the sialoglycans used in different studies. It emphasizes the need to better control the composition and to annotate it more clearly. In addition, different mice strains applied across multiple studies may exert distinct receptor function, expression and distribution. The ability of the tool antibody to bind to murine targets can further affect the clearance. Finally, the route and site of administration and dose may impact the distribution and disposition of the antibody and thus glycosylation-dependent immunogenicity and clearance, however, this varies across different reports. Therefore, results from such studies are difficult to compare.

The neonatal Fc receptor is highly important for the turnover of serum IgG thus determines the half live of antibodies. Fc glycosylation does not appear to impact interaction with FcRn (77, 88). Recent studies demonstrated little effects of glycosylation on FcRn binding with sialylation of IgG1 increasing, and deglycosylation and mannosylation decreasing interaction with FcRn (89-91). These minor effects do not appear to be relevant for the pharmacokinetic properties of the antibody because antibody deglycosylation has so far not been shown to affect the clearance (92-94). These reports are in line with the results obtained with aglycosylated RTX in BALB/c mice.

Relevance for immunogenicity mitigation

Because the effects of RTX mannosylation on immunogenicity obtained in human were concordant with that in mice there is sufficient evidence to conclude that antibody (IgG1) mannosylation has negative consequences on the immunogenicity but also on the clearance. Therefore, there is a risk that the efficacy and safety of the therapeutic antibody can be negatively affected. Nonetheless, the amount of high mannose in recombinant antibodies is usually low (although contents with up to 20 % have been reported (76)). Recommendations on an acceptable maximum content of high mannose cannot be made based on the results from this study. Comparisons of RTX containing sequentially rising mannose content (i.e. with 10 %, 20 %, 40 %, 60 %, 80 %, 100 % high mannose) would be needed to inform on any threshold.

Sialylation of antibodies may be a promising strategy to mitigate immunogenicity. Results from our study mostly rely on tolerogenic effects at the DC recognition and uptake axis *in vitro* in human. In order to gain further confidence that sialylation impacts the humoral immune response, studies using a relevant mouse model are required.

Conclusion

This work with RTX and specific engineered glycovariants demonstrates for the first time that antibody glycosylation (excluding non-human immunogenic glycan epitopes α 1-3gal and Neu5Gc) increases or decreases antigen recognition and impacts immunogenicity. Fc glycans facilitate the efficient uptake of antibodies in a receptor-dependent manner by DCs, and thus determine antigen routing into the degradative pathway, antigen presentation and effector T cell responses and ultimately humoral responses.

Whether the role of glycosylation on immunogenicity is generalizable beyond RTX, needs to be demonstrated using additional therapeutic antibodies.

Data Availability statement

Data available on request from the authors

Competing interests

All authors are employees of Novartis at the time of submission except for Stephan von Gunten who is employed at the University of Bern, Switzerland.

Funding statement

The laboratory of S.V.G is supported by grants from the Swiss National Science Foundation (SNSF) [310030_184757] and the Swiss Cancer League/Swiss Cancer Research [KFS-4958-02-2020].

Author contribution

Babette Wolf^{1,2,3,4,5}; Mateusz Piksa^{1,2,3,4}; Agnes Patoux^{1,3,4}; Isabelle Beley^{1,2,3,4}; Thierry Besson^{1,2,3}; Valerie Cordier^{1,2,3}; Bernd Voedisch^{2,4}; Daniela Stöllner^{2,4}; Ludovic Perrot²; Patrick Schindler²; Dominique Brees²; Stephan von Gunten^{2,5}; Michael Kammüller^{2,5}

¹performed the research, ²study design, ³data analysis, ⁴contributed essential tools and assays, ⁵wrote the paper

Acknowledgment

We thank Brigitte Christen, Jeannine Hehlen, Deborah Garcia, Nathalie Loll, Magdalena Westphal, Aline Piequet, Valerie Dubost and all other colleagues not named here who have supported the multiple studies performed or provided advice.

References

1. Chung CH, Mirakhur B, Chan E, Le Q-T, Berlin J, Morse M, et al. Cetuximab-induced anaphylaxis and IgE specific for galactose- α -1,3-galactose. *N Engl J Med*. 2008;358.
2. Ghaderi D, Taylor RE, Padler-Karavani V, Diaz S, Varki A. Implications of the presence of N-glycolylneuraminic acid in recombinant therapeutic glycoproteins. *Nat Biotech*. 2010;28(8):863-7.
3. Yu C, Gao K, Zhu L, Wang W, Wang L, Zhang F, et al. At least two Fc Neu5Gc residues of monoclonal antibodies are required for binding to anti-Neu5Gc antibody. *Scientific Reports*. 2016;6(1):20029.
4. Kaneko Y, Nimmerjahn F, Ravetch JV. Anti-inflammatory activity of immunoglobulin G resulting from Fc sialylation. *Science*. 2006;313(5787):670-3.
5. Dorokhov YL, Sheshukova EV, Kosobokova EN, Shindyapina AV, Kosorukov VS, Komarova TV. Functional role of carbohydrate residues in human immunoglobulin G and therapeutic monoclonal antibodies. *Biochemistry (Moscow)*. 2016;81(8):835-57.
6. Higel F, Sandl T, Kao C-Y, Pechinger N, Sörgel F, Friess W, et al. N-glycans of complex glycosylated biopharmaceuticals and their impact on protein clearance. *European Journal of Pharmaceutics and Biopharmaceutics*. 2019;139:123-31.
7. Schiestl M, Stangler T, Torella C, Cepeljnik T, Toll H, Grau R. Acceptable changes in quality attributes of glycosylated biopharmaceuticals. *Nature biotechnology*. 2011;29(4):310-2.
8. Dasgupta S, Navarrete A-M, Bayry J, Delignat S, Wootla B, André S, et al. A role for exposed mannosylations in presentation of human therapeutic self-proteins to CD4+ T lymphocytes. *Proceedings of the National Academy of Sciences of the United States of America*. 2007;104(21):8965-70.
9. Čaval T, Tian W, Yang Z, Clausen H, Heck AJR. Direct quality control of glycoengineered erythropoietin variants. *Nature Communications*. 2018;9(1):3342.
10. Du H, Levine M, Ganesa C, Witte DP, Cole ES, Grabowski GA. The Role of Mannosylated Enzyme and the Mannose Receptor in Enzyme Replacement Therapy. *The American Journal of Human Genetics*. 2005;77(6):1061-74.
11. Deisenhofer J. Crystallographic refinement and atomic models of a human Fc fragment and its complex with fragment B of protein A from *Staphylococcus aureus* at 2.9- and 2.8-Å resolution. *Biochemistry*. 1981;20(9):2361-70.
12. Zhou Q, Qiu H. The Mechanistic Impact of N-Glycosylation on Stability, Pharmacokinetics, and Immunogenicity of Therapeutic Proteins. *Journal of Pharmaceutical Sciences*. 2018.
13. Dubé S, Fisher JW, Powell JS. Glycosylation at specific sites of erythropoietin is essential for biosynthesis, secretion, and biological function. *The Journal of biological chemistry*. 1988;263(33):17516-21.
14. Beck A, Reichert JM. Marketing approval of mogamulizumab: A triumph for glyco-engineering. *mAbs*. 2012;4(4):419-25.
15. Reusch D, Tejada ML. Fc glycans of therapeutic antibodies as critical quality attributes. *Glycobiology*. 2015;25(12):1325-34.
16. Dong X, Storkus WJ, Salter RD. Binding and Uptake of Agalactosyl IgG by Mannose Receptor on Macrophages and Dendritic Cells. *The Journal of Immunology*. 1999;163(10):5427-34.
17. Dunn N, Juto A, Ryner M, Manouchehrinia A, Piccoli L, Fink K, et al. Rituximab in multiple sclerosis: Frequency and clinical relevance of anti-drug antibodies. *Multiple Sclerosis Journal*. 2017;24(9):1224-33.
18. Mok CC. Rituximab for the treatment of rheumatoid arthritis: an update. *Drug Design, Development and Therapy*. 2014;8:87-100.
19. Wincup C, Menon M, Smith E, Schwartz A, Isenberg D, Jury EC, et al. Presence of anti-rituximab antibodies predicts infusion-related reactions in patients with systemic lupus erythematosus. *Annals of the Rheumatic Diseases*. 2019;78(8):1140-2.
20. Chung C-Y, Wang Q, Yang S, Chough S, Seo Y, Cipollo JF, et al. The impact of sialylation linkage-type on the pharmacokinetics of recombinant butyrylcholinesterases. *Biotechnology and Bioengineering*. 2020;117(1):157-66.
21. Miranda-Hernández MP, López-Morales CA, Ramírez-Ibáñez ND, Piña-Lara N, Pérez NO, Molina-Pérez A, et al. Assessment of Physicochemical Properties of Rituximab Related to Its Immunomodulatory Activity. *Journal of immunology research*. 2015;2015:910763.
22. Lee KH, Lee J, Bae JS, Kim YJ, Kang HA, Kim SH, et al. Analytical similarity assessment of rituximab biosimilar CT-P10 to reference medicinal product. *MABs*. 2018;10(3):380-96.

23. Wang H, Wu L, Wang C, Xu J, Yin H, Guo H, et al. Biosimilar or Not: Physicochemical and Biological Characterization of MabThera and Its Two Biosimilar Candidates. *ACS Pharmacol Transl Sci.* 2021;4(2):790-801.
24. Jafari M, Ansari-Pour N. Why, When and How to Adjust Your P Values? *Cell J.* 2019;20(4):604-7.
25. Millward TA, Heitzmann M, Bill K, Längle U, Schumacher P, Forrer K. Effect of constant and variable domain glycosylation on pharmacokinetics of therapeutic antibodies in mice. *Biologicals.* 2008;36(1):41-7.
26. Zhang L, Luo S, Zhang B. The use of lectin microarray for assessing glycosylation of therapeutic proteins. *MAbs.* 2016;8(3):524-35.
27. Fukumori F, Takeuchi N, Hagiwara T, Ohbayashi H, Endo T, Kochibe N, et al. Primary Structure of a Fucose-Specific Lectin Obtained from a Mushroom, *Aleuria aurantia*. *The Journal of Biochemistry.* 1990;107(2):190-6.
28. Wu AM, Wu JH, Singh T, Lai L-J, Yang Z, Herp A. Recognition factors of Ricinus communis agglutinin 1 (RCA1). *Molecular Immunology.* 2006;43(10):1700-15.
29. Naismith JH, Field RA. Structural basis of trimannoside recognition by concanavalin A. *The Journal of biological chemistry.* 1996;271(2):972-6.
30. Crowley JF, Goldstein IJ, Arnarp J, Lönngren J. Carbohydrate binding studies on the lectin from *Datura stramonium* seeds. *Archives of biochemistry and biophysics.* 1984;231(2):524-33.
31. Ritchie M, Tchistiakova L, Scott N. Implications of receptor-mediated endocytosis and intracellular trafficking dynamics in the development of antibody drug conjugates. *mAbs.* 2013;5(1):13-21.
32. García-Vallejo JJ, Van Kooyk Y. Endogenous ligands for C-type lectin receptors: the true regulators of immune homeostasis. *Immunological Reviews.* 2009;230(1):22-37.
33. Streng-Ouwehand I, Ho NI, Litjens M, Kalay H, Boks MA, Cornelissen LAM, et al. Glycan modification of antigen alters its intracellular routing in dendritic cells, promoting priming of T cells. *eLife.* 2016;5:e11765.
34. Baker K, Rath T, Pyzik M, Blumberg RS. The Role of FcRn in Antigen Presentation. *Frontiers in Immunology.* 2014;5:408.
35. Bournazos S, Wang TT, Ravetch JV. The Role and Function of Fcγ Receptors on Myeloid Cells. *Microbiology Spectrum.* 2016;4(6).
36. Boruchov AM, Heller G, Veri M-C, Bonvini E, Ravetch JV, Young JW. Activating and inhibitory IgG Fc receptors on human DCs mediate opposing functions. *Journal of Clinical Investigation.* 2005;115(10):2914-23.
37. Engering A, Geijtenbeek TBH, van Vliet SJ, Wijers M, van Liempt E, Demaurex N, et al. The Dendritic Cell-Specific Adhesion Receptor DC-SIGN Internalizes Antigen for Presentation to T Cells. *The Journal of Immunology.* 2002;168(5):2118-26.
38. Vendele I, Willment JA, Silva LM, Palma AS, Chai W, Liu Y, et al. Mannan detecting C-type lectin receptor probes recognise immune epitopes with diverse chemical, spatial and phylogenetic heterogeneity in fungal cell walls. *PLoS Pathog.* 2020;16(1):e1007927-e.
39. Nicoll G, Ni J, Liu D, Klenerman P, Munday J, Dubock S, et al. Identification and Characterization of a Novel Siglec, Siglec-7, Expressed by Human Natural Killer Cells and Monocytes. *Journal of Biological Chemistry.* 1999;274(48):34089-95.
40. Angata T, Varki A. Siglec-7: a sialic acid-binding lectin of the immunoglobulin superfamily. *Glycobiology.* 2000;10(4):431-8.
41. Liming L. Antibody Glycosylation and Its Impact on the Pharmacokinetics and Pharmacodynamics of Monoclonal Antibodies and Fc-Fusion Proteins. *Journal of Pharmaceutical Sciences.* 2015;104(6):1866-84.
42. Luo C, Chen S, Xu N, Wang C, Sai Wb, Zhao W, et al. Glycoengineering of pertuzumab and its impact on the pharmacokinetic/pharmacodynamic properties. *Scientific Reports.* 2017;7:46347.
43. Ryman JT, Meibohm B. Pharmacokinetics of Monoclonal Antibodies. *CPT: Pharmacometrics & Systems Pharmacology.* 2017;6(9):576-88.
44. Chirmule N, Jawa V, Meibohm B. Immunogenicity to Therapeutic Proteins: Impact on PK/PD and Efficacy. *The AAPS Journal.* 2012;14(2):296-302.
45. Kamath AV. Translational pharmacokinetics and pharmacodynamics of monoclonal antibodies. *Drug Discovery Today: Technologies.*

46. Smith A, Manoli H, Jaw S, Frutoz K, Epstein AL, Khawli LA, et al. Unraveling the Effect of Immunogenicity on the PK/PD, Efficacy, and Safety of Therapeutic Proteins. *Journal of immunology research*. 2016;2016:2342187.
47. Wawrzyniak M, Morsy Y, Mladenov R, Tontodonati G, Turgay Y, Herwig S, et al. Fucosylation and Sialylation of Fc-Fragment of anti-Tumour Necrosis Factor Alpha Antibodies do not Influence Their Immunogenicity in Monocyte-Derived Dendritic Cells. *J Crohns Colitis*. 2021;15(9):1596-601.
48. Drickamer K. Engineering galactose-binding activity into a C-type mannose-binding protein. *Nature*. 1992;360(6400):183-6.
49. Engering AJ, Cella M, Fluitsma D, Brockhaus M, Hoefsmit EC, Lanzavecchia A, et al. The mannose receptor functions as a high capacity and broad specificity antigen receptor in human dendritic cells. *European journal of immunology*. 1997;27(9):2417-25.
50. Lee RT, Hsu T-L, Huang SK, Hsieh S-L, Wong C-H, Lee YC. Survey of immune-related, mannose/fucose-binding C-type lectin receptors reveals widely divergent sugar-binding specificities. *Glycobiology*. 2010;21(4):512-20.
51. Lu LL, Suscovich TJ, Fortune SM, Alter G. Beyond binding: antibody effector functions in infectious diseases. *Nature Reviews Immunology*. 2018;18(1):46-61.
52. Anthony RM, Kobayashi T, Wermeling F, Ravetch JV. Intravenous gammaglobulin suppresses inflammation through a novel T(H)2 pathway. *Nature*. 2011;475(7354):110-3.
53. Yu X, Vasiljevic S, Mitchell DA, Crispin M, Scanlan CN. Dissecting the molecular mechanism of IVIg therapy: the interaction between serum IgG and DC-SIGN is independent of antibody glycoform or Fc domain. *J Mol Biol*. 2013;425(8):1253-8.
54. Bayry J, Bansal K, Kazatchkine MD, Kaveri SV. DC-SIGN and alpha2,6-sialylated IgG Fc interaction is dispensable for the anti-inflammatory activity of IVIg on human dendritic cells. *Proceedings of the National Academy of Sciences of the United States of America*. 2009;106(9):E24-E5.
55. Lam JS, Huang H, Levitz SM. Effect of Differential N-linked and O-linked Mannosylation on Recognition of Fungal Antigens by Dendritic Cells. *PLOS ONE*. 2007;2(10):e1009.
56. Burgdorf S, Lukacs-Kornek V, Kurts C. The mannose receptor mediates uptake of soluble but not of cell-associated antigen for cross-presentation. *Journal of immunology (Baltimore, Md : 1950)*. 2006;176(11):6770-6.
57. Mahnke K, Guo M, Lee S, Sepulveda H, Swain SL, Nussenzweig M, et al. The dendritic cell receptor for endocytosis, DEC-205, can recycle and enhance antigen presentation via major histocompatibility complex class II-positive lysosomal compartments. *J Cell Biol*. 2000;151(3):673-84.
58. Perdicchio M, Ilarregui JM, Verstege MI, Cornelissen LAM, Schetters STT, Engels S, et al. Sialic acid-modified antigens impose tolerance via inhibition of T-cell proliferation and de novo induction of regulatory T cells. *Proceedings of the National Academy of Sciences of the United States of America*. 2016;113(12):3329-34.
59. Hiltbold EM, Vlad AM, Ciborowski P, Watkins SC, Finn OJ. The mechanism of unresponsiveness to circulating tumor antigen MUC1 is a block in intracellular sorting and processing by dendritic cells. *Journal of immunology (Baltimore, Md : 1950)*. 2000;165(7):3730-41.
60. Botarelli P, Houlden BA, Haigwood NL, Servis C, Montagna D, Abrignani S. N-glycosylation of HIV-gp120 may constrain recognition by T lymphocytes. *Journal of immunology (Baltimore, Md : 1950)*. 1991;147(9):3128-32.
61. Drummer HE, Jackson DC, Brown LE. Modulation of CD4+ T-Cell Recognition of Influenza Hemagglutinin by Carbohydrate Side Chains Located Outside a T-Cell Determinant. *Virology*. 1993;192(1):282-9.
62. Hamze M, Meunier S, Karle A, Gdoura A, Goudet A, Szely N, et al. Characterization of CD4 T Cell Epitopes of Infliximab and Rituximab Identified from Healthy Donors. *Frontiers in Immunology*. 2017;8(500).
63. Cornaby C, Gibbons L, Mayhew V, Sloan CS, Welling A, Poole BD. B cell epitope spreading: Mechanisms and contribution to autoimmune diseases. *Immunology Letters*. 2015;163(1):56-68.
64. Housseau F, Moorthy A, Langer DA, Robbins PF, Gonzales MI, Topalian SL. N-linked carbohydrates in tyrosinase are required for its recognition by human MHC class II-restricted CD4(+) T cells. *European journal of immunology*. 2001;31(9):2690-701.
65. Dudler T, Altmann F, Carballido JM, Blaser K. Carbohydrate-dependent, HLA class II-restricted, human T cell response to the bee venom allergen phospholipase A2 in allergic patients. *European journal of immunology*. 1995;25(2):538-42.

66. Bäcklund J, Carlsen S, Höger T, Holm B, Fugger L, Kihlberg J, et al. Predominant selection of T cells specific for the glycosylated collagen type II epitope (263–270) in humanized transgenic mice and in rheumatoid arthritis. *Proceedings of the National Academy of Sciences*. 2002;99(15):9960-5.
67. Lakshminarayanan V, Thompson P, Wolfert MA, Buskas T, Bradley JM, Pathangey LB, et al. Immune recognition of tumor-associated mucin MUC1 is achieved by a fully synthetic aberrantly glycosylated MUC1 tripartite vaccine. *Proceedings of the National Academy of Sciences*. 2012;109(1):261-6.
68. von Mensdorff-Pouilly S, Petrakou E, Kenemans P, van Uffelen K, Verstraeten AA, Snijdwint FG, et al. Reactivity of natural and induced human antibodies to MUC1 mucin with MUC1 peptides and n-acetylgalactosamine (GalNAc) peptides. *International journal of cancer*. 2000;86(5):702-12.
69. Wolfert MA, Boons G-J. Adaptive immune activation: glycosylation does matter. *Nature chemical biology*. 2013;9(12):776-84.
70. Akdis M, Aab A, Altunbulakli C, Azkur K, Costa RA, Cramer R, et al. Interleukins (from IL-1 to IL-38), interferons, transforming growth factor β , and TNF- α : Receptors, functions, and roles in diseases. *Journal of Allergy and Clinical Immunology*. 2016;138(4):984-1010.
71. Blink SE, Fu Y-X. IgE regulates T helper cell differentiation through Fc γ RIII mediated dendritic cell cytokine modulation. *Cell Immunol*. 2010;264(1):54-60.
72. Bruhns P, Iannascoli B, England P, Mancardi DA, Fernandez N, Jorieux S, et al. Specificity and affinity of human Fc γ receptors and their polymorphic variants for human IgG subclasses 2009 2009-04-16 00:00:00. 3716-25 p.
73. Bruhns P. Properties of mouse and human IgG receptors and their contribution to disease models. *Blood*. 2012;119(24):5640-9.
74. Lux A, Nimmerjahn F. Of Mice and Men: The Need for Humanized Mouse Models to Study Human IgG Activity in Vivo. *Journal of Clinical Immunology*. 2013;33(1):4-8.
75. Overdijk MB, Verploegen S, Ortiz Buijsse A, Vink T, Leusen JHW, Bleeker WK, et al. Crosstalk between Human IgG Isotypes and Murine Effector Cells. *The Journal of Immunology*. 2012;189(7):3430-8.
76. Goetze AM, Liu YD, Zhang Z, Shah B, Lee E, Bondarenko PV, et al. High-mannose glycans on the Fc region of therapeutic IgG antibodies increase serum clearance in humans. *Glycobiology*. 2011;21(7):949-59.
77. Kanda Y, Yamada T, Mori K, Okazaki A, Inoue M, Kitajima-Miyama K, et al. Comparison of biological activity among nonfucosylated therapeutic IgG1 antibodies with three different N-linked Fc oligosaccharides: the high-mannose, hybrid, and complex types. *Glycobiology*. 2007;17(1):104-18.
78. Wright A, Morrison SL. Effect of altered CH2-associated carbohydrate structure on the functional properties and in vivo fate of chimeric mouse-human immunoglobulin G1. *The Journal of Experimental Medicine*. 1994;180(3):1087-96.
79. Yu M, Brown D, Reed C, Chung S, Lutman J, Stefanich E, et al. Production, characterization and pharmacokinetic properties of antibodies with N-linked Mannose-5 glycans. *mAbs*. 2012;4(4):475-87.
80. Chen X, Liu YD, Flynn GC. The effect of Fc glycan forms on human IgG2 antibody clearance in humans. *Glycobiology*. 2009;19(3):240-9.
81. BOVENSCHEN N, RIJKEN DC, HAVEKES LM, VAN VLIJMEN BJM, MERTENS K. The B domain of coagulation factor VIII interacts with the asialoglycoprotein receptor. *Journal of Thrombosis and Haemostasis*. 2005;3(6):1257-65.
82. Furbish FS, Steer CJ, Barranger JA, Jones EA, Brady RO. The uptake of native and desialylated glucocerebrosidase by rat hepatocytes and Kupffer cells. *Biochemical and Biophysical Research Communications*. 1978;81(3):1047-53.
83. Liu L, Li H, Hamilton SR, Gomathinayagam S, Rayfield WJ, van Maanen M, et al. The Impact of Sialic Acids on the Pharmacokinetics of a PEGylated Erythropoietin. *Journal of Pharmaceutical Sciences*. 2012;101(12):4414-8.
84. Morell AG, Gregoriadis G, Scheinberg IH, Hickman J, Ashwell G. The role of sialic acid in determining the survival of glycoproteins in the circulation. *The Journal of biological chemistry*. 1971;246(5):1461-7.
85. Bas M, Terrier A, Jacque E, Dehenne A, Pochet-Béghin V, Béghin C, et al. Fc Sialylation Prolongs Serum Half-Life of Therapeutic Antibodies. *Journal of immunology (Baltimore, Md : 1950)*. 2019;202(5):1582-94.
86. Naso MF, Tam SH, Scallon BJ, Raju TS. Engineering host cell lines to reduce terminal sialylation of secreted antibodies. *mAbs*. 2010;2(5):519-27.

87. Park EI, Mi Y, Unverzagt C, Gabius H-J, Baenziger JU. The asialoglycoprotein receptor clears glycoconjugates terminating with sialic acid α 2,6GalNAc. *Proceedings of the National Academy of Sciences of the United States of America*. 2005;102(47):17125-9.
88. Jefferis R. Isotype and glycoform selection for antibody therapeutics. *Archives of biochemistry and biophysics*. 2012;526(2):159-66.
89. Cymer F, Beck H, Rohde A, Reusch D. Therapeutic monoclonal antibody N-glycosylation – Structure, function and therapeutic potential. *Biologicals*. 2018;52:1-11.
90. Dashivets T, Thomann M, Rueger P, Knaupp A, Buchner J, Schlothauer T. Multi-Angle Effector Function Analysis of Human Monoclonal IgG Glycovariants. *PLOS ONE*. 2015;10(12):e0143520.
91. Wada R, Matsui M, Kawasaki N. Influence of N-glycosylation on effector functions and thermal stability of glycoengineered IgG1 monoclonal antibody with homogeneous glycoforms. *MAbs*. 2019;11(2):350-72.
92. Leabman MK, Meng YG, Kelley RF, DeForge LE, Cowan KJ, Iyer S. Effects of altered Fc γ R binding on antibody pharmacokinetics in cynomolgus monkeys. *mAbs*. 2013;5(6):896-903.
93. Liu L, Stadheim A, Hamuro L, Pittman T, Wang W, Zha D, et al. Pharmacokinetics of IgG1 monoclonal antibodies produced in humanized *Pichia pastoris* with specific glycoforms: a comparative study with CHO produced materials. *Biologicals*. 2011;39(4):205-10.
94. Tao MH, Morrison SL. Studies of aglycosylated chimeric mouse-human IgG. Role of carbohydrate in the structure and effector functions mediated by the human IgG constant region. *The Journal of Immunology*. 1989;143(8):2595-601.

References R packages

- RStudio Team (2020). *_RStudio: Integrated Development Environment for R_*. RStudio, Inc., Boston, MA. <http://www.rstudio.com>.
- R Core Team (2020). *_R: A Language and Environment for Statistical Computing_*. R Foundation for Statistical Computing, Vienna, Austria. <https://www.R-project.org>.
- Wickham H, Seidel D (2019). *_scales: Scale Functions for Visualization_*. R package version 1.1.0, <https://CRAN.R-project.org/package=scales>.
- Gohel D (2020). *_flextable: Functions for Tabular Reporting_*. R package version 0.5.11, <https://CRAN.R-project.org/package=flextable>.
- Wei T, Simko V (2017). *_R package "corrplot": Visualization of a Correlation Matrix_*. (Version 0.84), <https://github.com/taiyun/corrplot>.
- Gagolewski M (2020). *_R package stringi: Character string processing facilities_*. <http://www.gagolewski.com/software/stringi/>.
- Wickham H (2019). *_stringr: Simple, Consistent Wrappers for Common String Operations_*. R package version 1.4.0, <https://CRAN.R-project.org/package=stringr>.
- Pedersen T (2020). *_ggforce: Accelerating 'ggplot2'_*. R package version 0.3.2, <https://CRAN.R-project.org/package=ggforce>.
- Harrell Jr FE, Dupont wcfC, others. m (2020). *_Hmisc: Harrell Miscellaneous_*. R package version 4.4-0, <https://CRAN.R-project.org/package=Hmisc>.
- Zeileis A, Croissant Y (2010). "Extended Model Formulas in R: Multiple Parts and Multiple Responses." *_Journal of Statistical Software_*, *34*(1), 1-13. doi: 10.18637/jss.v034.i01 <https://doi.org/10.18637/jss.v034.i01>.
- Sarkar D (2008). *_Lattice: Multivariate Data Visualization with R_*. Springer, New York. ISBN 978-0-387-75968-5, <http://lmdvr.r-forge.r-project.org>.
- Robinson D, Hayes A (2020). *_broom: Convert Statistical Analysis Objects into Tidy Tibbles_*. R package version 0.5.6, <https://CRAN.R-project.org/package=broom>.
- Kassambara A (2020). *_ggpubr: 'ggplot2' Based Publication Ready Plots_*. R package version 0.3.0, <https://CRAN.R-project.org/package=ggpubr>.
- Fox J, Weisberg S (2019). *_An R Companion to Applied Regression_*, Third edition. Sage, Thousand Oaks CA. <https://socialsciences.mcmaster.ca/jfox/Books/Companion>.
- Fox J, Weisberg S, Price B (2019). *_carData: Companion to Applied Regression Data Sets_*. R package version 3.0-3, <https://CRAN.R-project.org/package=carData>.

- Ahlmann-Eltze C (2019). `_ggsignif`: Significance Brackets for 'ggplot2'. R package version 0.6.0, <https://CRAN.R-project.org/package=ggsignif>.
- al. ASem (2020). `_DescTools`: Tools for Descriptive Statistics. R package version 0.99.36, <https://cran.r-project.org/package=DescTools>.
- Wickham H (2007). "Reshaping Data with the reshape Package." *Journal of Statistical Software*, *21*(12), 1-20. <http://www.jstatsoft.org/v21/i12/>.
- Wickham H (2016). `_ggplot2`: Elegant Graphics for Data Analysis. Springer-Verlag New York. ISBN978-3-319-24277-4, <https://ggplot2.tidyverse.org>.
- Wickham H, Henry L (2020). `_tidyr`: Tidy Messy Data. R package version 1.0.2, <https://CRAN.R-project.org/package=tidyr>.
- Wickham H, François R, Henry L, Müller K (2020). `_dplyr`: A Grammar of Data Manipulation. R package version 1.0.0, <https://CRAN.R-project.org/package=dplyr>.
- Ooms J (2019). `_writexl`: Export Data Frames to Excel 'xlsx' Format. R package version 1.2, <https://CRAN.R-project.org/package=writexl>.
- Wickham H, Bryan J (2019). `_readxl`: Read Excel Files. R package version 1.3.1, <https://CRAN.R-project.org/package=readxl>

Figure Legends

Figure 1: RTX Fc N-glycans can be recognized by lectins.

A: Theoretical lectin recognition motifs on rituximab (RTX) WT (unmodified) Fc N-glycans; AAL: Aleuria aurantia lectin (specific to core fucose), ConA: Concanavalin A (specific to Man α 1-6(Man α 1-3)Man), DSA: Datura stramonium agglutinin (specific to GlcNAc β 1-4), RCA: Ricinus communis agglutinin (specific to Gal β 1-4GlcNAc); B: Binding of biotinylated lectins to RTX WT Fc N-glycans was assessed by ELISA: -Lec: Control without biotinylated lectin, aglycosylated (N297A) RTX served as negative control in addition to the medium control (Med); C: Competition ELISA with Methylmannoside (MM) for ConA and Galactose (Gal) for RCA; mean of technical duplicates of a representative experiment, error bars: SD

Figure 2: Glycosylation facilitates and impacts binding and internalization by DCs

A: DC-internalization of unmodified (WT), aglycosylated (N297A), mannosylated (HiMan) and hypersialylated (HySi) rituximab (RTX) as measured by FACS at 60 min. % Internalization was calculated from the difference of the percentage of bound (4°C) and internalized (37°C) RTX on viable IDCs, n = 6 human donors, one data point represents the mean of technical duplicates, statistical analysis performed by pairwise Wilcoxon test; B: Target-binding of RTX glycovariants to CD20-positive Ramos cells is not affected by glycosylation, mean of technical duplicates from one representative experiment, Med: Medium control; Confocal images (40x) of IDCs from one human donor after binding at 4°C (C) and internalization at 37°C (D) of AF647-conjugated RTX glycovariants (red), nuclear stain: DAPI (blue); E: Quantification of intracellular RTX staining from confocal images as shown in D after DC uptake of RTX glycovariants at 37°C calculated with HALO™ image analysis software (Akoya Biosciences®), n = 3 images per variant from ~120 cells per image.

Figure 3: RTX glycosylation influences routing into the degradative pathway

Images (40x) of immature dendritic cells (IDCs) from one treatment-naive human donor after internalization of AF647-conjugated rituximab (RTX) glycovariants (red) co-localized with marker antibodies (green) for A: Lamp1 (lysosome), B: EEA1 (early endosome) or C: Rab7 (late endosome) detected by confocal microscopy; Quantification of co-localized RTX with respective endolysosomal markers calculated with HALOTM

image analysis software (Akoya Biosciences®) from ~120 cells per image are shown right to the images. WT: unmodified, N297A: aglycosylated, HiMan: mannosylated, HySi: hypersialylated

Figure 4: *Antibody glycosylation impacts T cell activation which is associated with internalization*

Internalization and T cell response was assessed in the same donor set. A: Internalization of rituximab (RTX) glycovariants by immature dendritic cells (IDCs) using the IncuCyte Real Time Imager (median from 13 - 16 human treatment-naive donors, Integrated Intensity: fluorescence signal derived from AF647-labelled RTX glycovariants indicating internalization) measured at 2h, one data point represents the mean of technical duplicates of one donor, statistical analysis performed by pairwise Wilcox test; B: Absolute count of proliferating (cells/mL) and CD25+ Th cells determined from PBMCs of 13 - 16 human treatment-naive donors (same donor set as in A) primed and challenged with of each the RTX glycovariant (10 µg/mL); C: Stimulation indices calculated as ratio induced by the challenge relative to the prime response, donors were split into WT and non-WT responders; D: Response index for T cell assay in the same donor set, responding donor: donor with stimulation index above 1.5 (dashed line); E: Linear regression analysis for DC-internalization and T cell response induced by RTX glycovariants; WT: unmodified, N297A: aglycosylated, HiMan: mannosylated, HySi: hypersialylated

Figure 5: *RTX glycosylation affects T cell recognition*

A: Absolute count (cells/mL) of proliferating and CD25+ Th cells was determined from PBMCs of 10 human treatment-naive donors primed with WT RTX (rituximab) and challenged with RTX glycovariants (10 µg/mL); B: Stimulation indices calculated as ratio induced by the challenge relative to the priming response; C: Tested naive human donors (n = 10) were split into WT and non-WT responders; WT: unmodified, N297A: aglycosylated, HiMan: mannosylated, HySi: hypersialylated

Figure 6: *FcγRs and LRs mediate glycosylation-dependent DC internalization*

Internalization of rituximab (RTX) glycovariants by immature dendritic cells (IDCs) determined by indirect FACS assay at 60 min in presence of A: full-length IgG, n = 2 donors, or B: CD32-directed F(ab)² at 5 – 20 µg/mL, n = 2 donors; Inhibition of

internalization of RTX glycovariants determined by the IncuCyte real time imager assay at 3h in presence/absence of C: 5 mg/mL mannan, n = 5 donors; D: 20 ug/mL recombinant human DC-SIGN or 20 ug/mL recombinant human CD206 (=MR), n = 5 donors. E: 20 ug/mL recombinant human Siglec 7, n = 3 donors; Wo block: no ligand/recombinant receptor added, block: ligand or recombinant receptor added; numbers in the plots indicate p-values obtained from Tukey HSD; one data point represents the mean of technical duplicates of one donor; WT: unmodified, N297A: aglycosylated, HiMan: mannosylated, HySi: hypersialylated

Figure 7: Rituximab glycosylation impacts B and T cell immunogenicity and clearance in BALB/c mice

BALB/c mice received 6 subcutaneous (s.c.) injections of 0.5 mg/kg rituxmab (RTX) glycovariants or vehicle (Control) on D1, D4, D8, D11, D15 and D18. Anti-RTX antibodies (ADAs) of IgG isotype determined in serum of A: BALB/c mice collected on D-13 (pre) and before s.c. injection of 0.5 mg/kg RTX glycovariants or vehicle control (Control) on D4, D8, D11, D15 and D18, n = 10 mice; ADAs after 6 doses of RTX glycovariants (D18); statistical analysis performed by pairwise Wilcox test; B: BALB/c mice (n = 4) were immunized by s.c. injection of 0.5 mg/kg RTX WT + alum or alum only (Control). Th cell activation and proliferation in the treatment group (immunized with RTX WT) after ex vivo recall of splenocytes with 1 µg/mL of RTX glycovariant or 1 µg/mL ConA; stimulation index (SI) calculated as ratio of the treatment (WT or ConA) to medium response, dashed line: response threshold at SI of 1.5; C: Serum RTX after 1 dose at D1 4h (left) and 6 doses on D18 4h (right). Statistical analysis performed by pairwise Wilcox test; one data point represents the mean of technical duplicates of one animal; D: Regression analysis on the relationship of immunogenicity (anti-RTX antibodies) and exposure (serum RTX); WT: unmodified, N297A: aglycosylated, HiMan: mannosylated, HySi: hypersialylated

Figure 8: RTX glycosylation impacts cytokine response pattern in BALB/c mice

Fold changes in serum cytokines determined on D1 and D18 4h post dose in BALB/c mice immunized by bi-weekly s.c. injections of 0.5 mg/kg RTX (rituximab) glycovariants relative to pre-dose, n = 10 mice, one data point represents cytokine results from technical singlicates from one animal due to serum volume limitations; WT: unmodified, N297A: aglycosylated, HiMan: mannosylated, HySi: hypersialylated

Supplementary Figure 1: Glycan profile RTX glycovariants

Glycan profile for rituximab (RTX) glycovariants was determined by LC-MS (liquid chromatography coupled mass spectrometry) after IdeS (streptococcal Ig-degrading enzyme) reduction. Percentage of glycan species is reported in the table.

M5 – M9: 5 – 9 mannose glycan (high mannose)

G0F: fucosylated, agalactosylated complex type glycan

G1F: fucosylated, mono-galactosylated complex type glycan

G2F: fucosylated, di-galactosylated complex type glycan

G1FS1: fucosylated, mono-galactosylated, mono-sialylated complex type glycan

G2S1: di-galactosylated, mono-sialylated complex type glycan

G2FS1: fucosylated, di-galactosylated, mono-sialylated complex type glycan

G2FS2: fucosylated, di-galactosylated, di-sialylated complex type glycan

WT: unmodified rituximab (RTX), HiMan: mannosylated RTX, HySi: hypersialylated RTX

GlcNAc: N-acetylglucosamine, Man: mannose, Gal: galactose, NeuAc: N-acetylneuraminic acid = Sia = sialic acid, Fuc: fucose

Supplementary Figure 2: IncuCyte images of internalization of RTX glycovariants

A: Assay principle indirect FACS-based internalization assay and exemplary FSC-SSC plots and overlay plots of the binding (4°C) and internalization (37°C) of rituximab (RTX) glycovariants by immature dendritic cells (IDCs) of one representative donor. %Internalization as depicted in Figure 2A is calculated from the normalized percentage binding signal difference between 4°C and 37°C. A secondary FITC-labelled anti-RTX antibody was used to detect surface bound RTX, hence increased FITC-signal measured at 37°C corresponds to decreased internalization. B: Kinetic of internalization of RTX glycovariants by IDCs using the IncuCyte Real Time Imager (median from 16 human treatment-naive donors, Median Intensity: fluorescence signal derived from AF647-labelled RTX glycovariants indicating internalization); C: Representative images of internalization of AF647-labelled RTX glycovariants from a donor with increased internalization of N297A over WT or from a donor with increased internalization of WT over N297A at 3h time point measured with the IncuCyte Real Time analyzer; Med:

medium control or unstained; WT: unmodified, N297A: aglycosylated, HiMan: mannosylated, HySi: hypersialylated

Supplementary Figure 3: T cell assay dot plots from RTX glycovariants and controls

A: Representative dot plots of proliferating CD25+ Th cells induced by rituximab (RTX) glycovariant stimulation (10 µg/mL) with (+) or without (-) challenge (=prime response) from one human donor; B: Absolute counts of proliferating and CD25+ Th cells induced by medium, KLH (5 µg/mL) or tetanus toxoid (TT, 0.5 µg/mL) for all tested donors (n = 13 – 16) and representative dot plots from one donor; WT: unmodified, N297A: aglycosylated, HiMan: mannosylated, HySi: hypersialylated

Supplementary Figure 4: Correlation of LR and FcγR receptor expression and glycosylation-dependent internalization of RTX

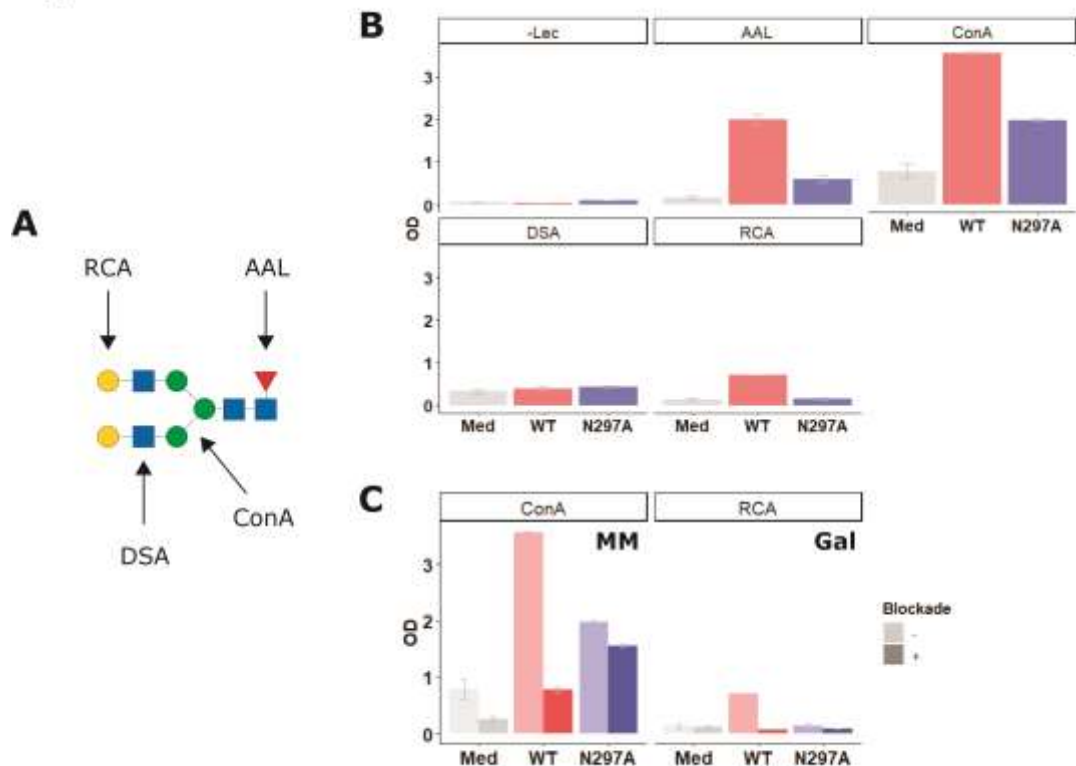
A: Lectin receptor (LR) and FcγR expression determined on immature dendritic cells (IDCs) from 13 - 16 human donors; B: Internalization of rituximab (RTX) glycovariants measured by IncuCyte at 2h in the same human donor set, statistical analysis performed by pairwise Wilcox test; C: Correlation matrix with correlation coefficients (Pearson) displaying the relationship between LR and FcγR expression and internalization of RTX glycovariants (red box); Med: medium control, WT: unmodified, N297A: aglycosylated, HiMan: mannosylated, HySi: hypersialylated

Therapeutic antibody glycosylation impacts antigen recognition and immunogenicity

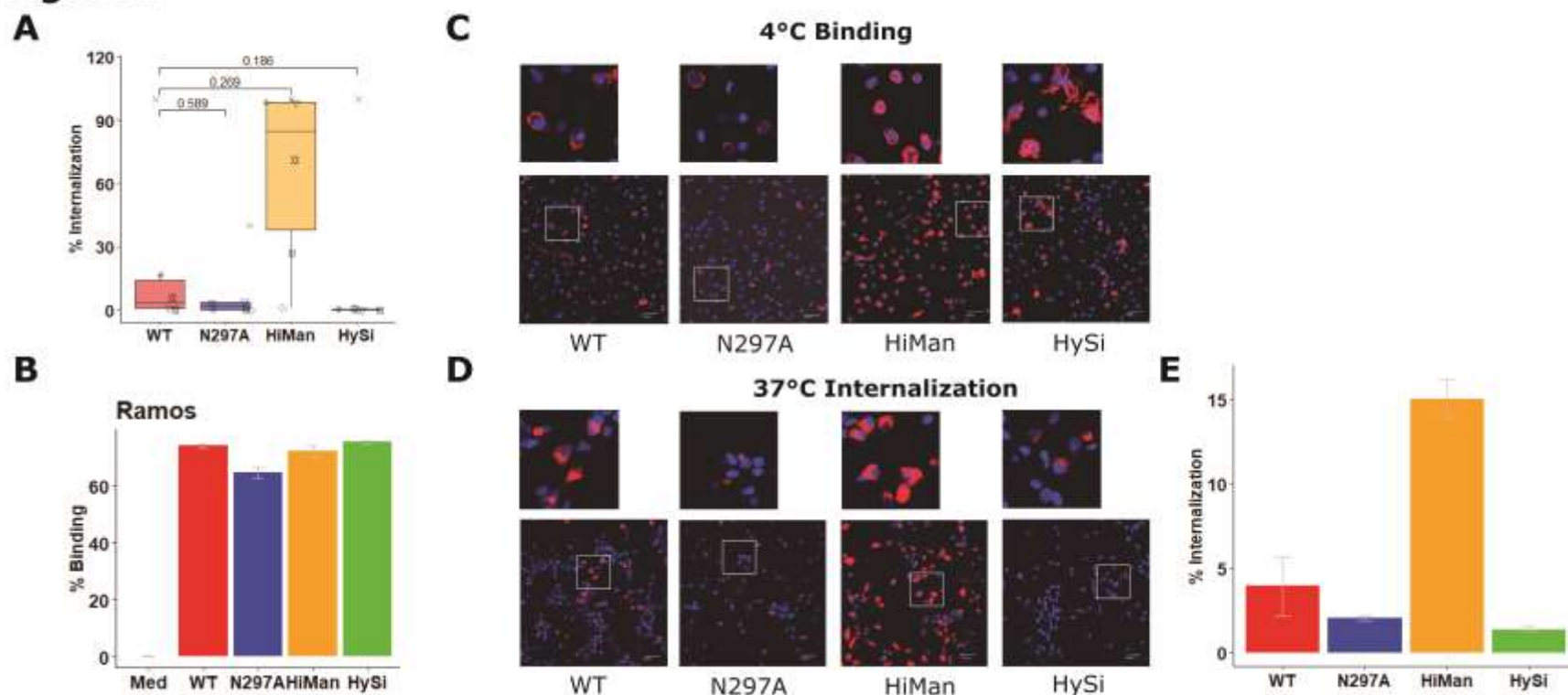
Babette Wolf¹, Mateusz Piksa¹, Isabelle Beley¹, Agnes Patoux¹, Thierry Besson¹, Valerie Cordier¹, Bernd Voedisch¹, Patrick Schindler¹, Daniela Stöllner¹, Ludovic Perrot¹, Stephan von Gunten², Dominique Brees¹, Michael Kammüller¹

¹Novartis Institutes for BioMedical Research, Basel, Switzerland

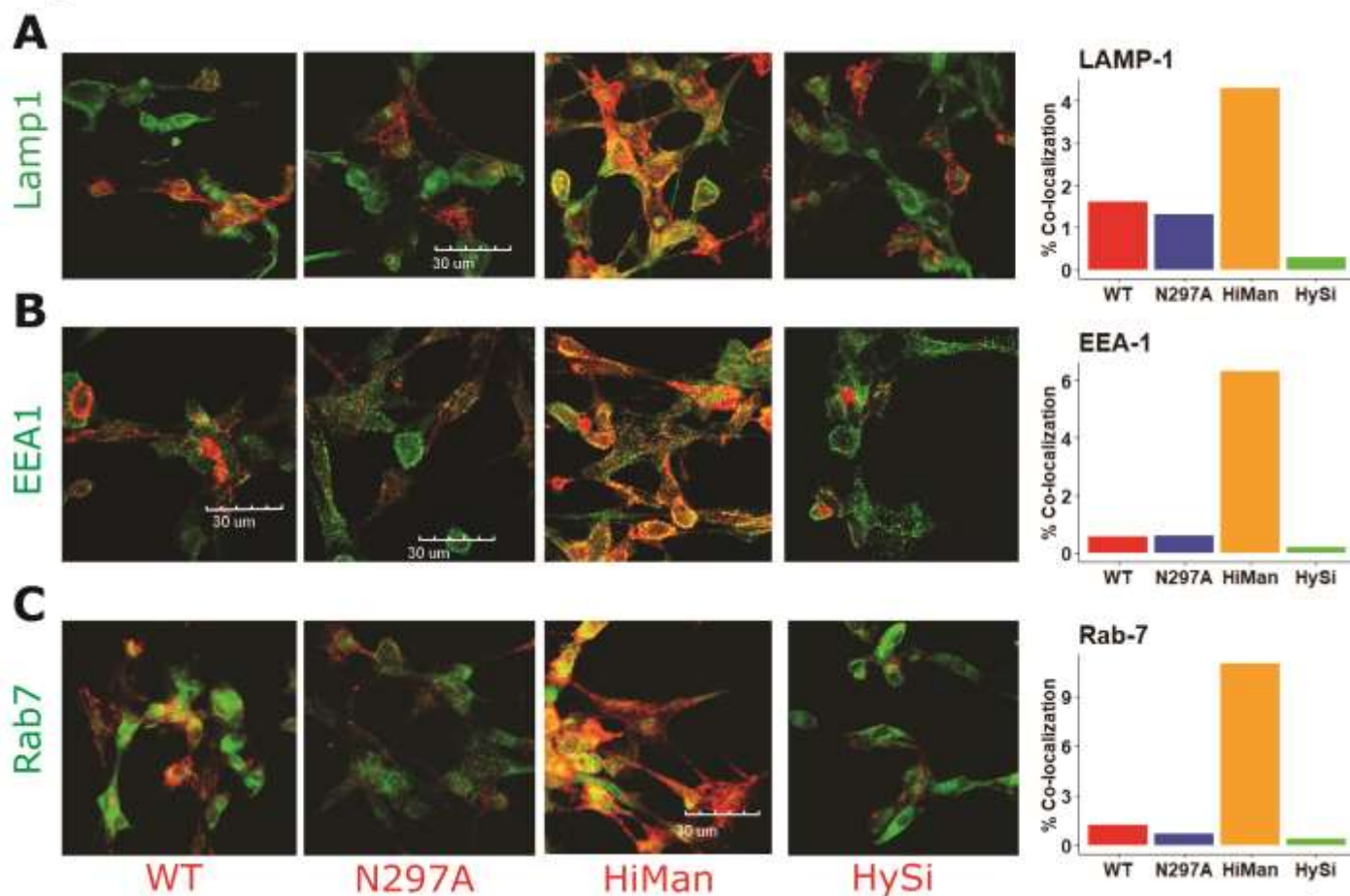
²Institute of Pharmacology, University of Bern, Bern, Switzerland

Figure 1**Figure 1:** RTX Fc N-glycans can be recognized by lectins.

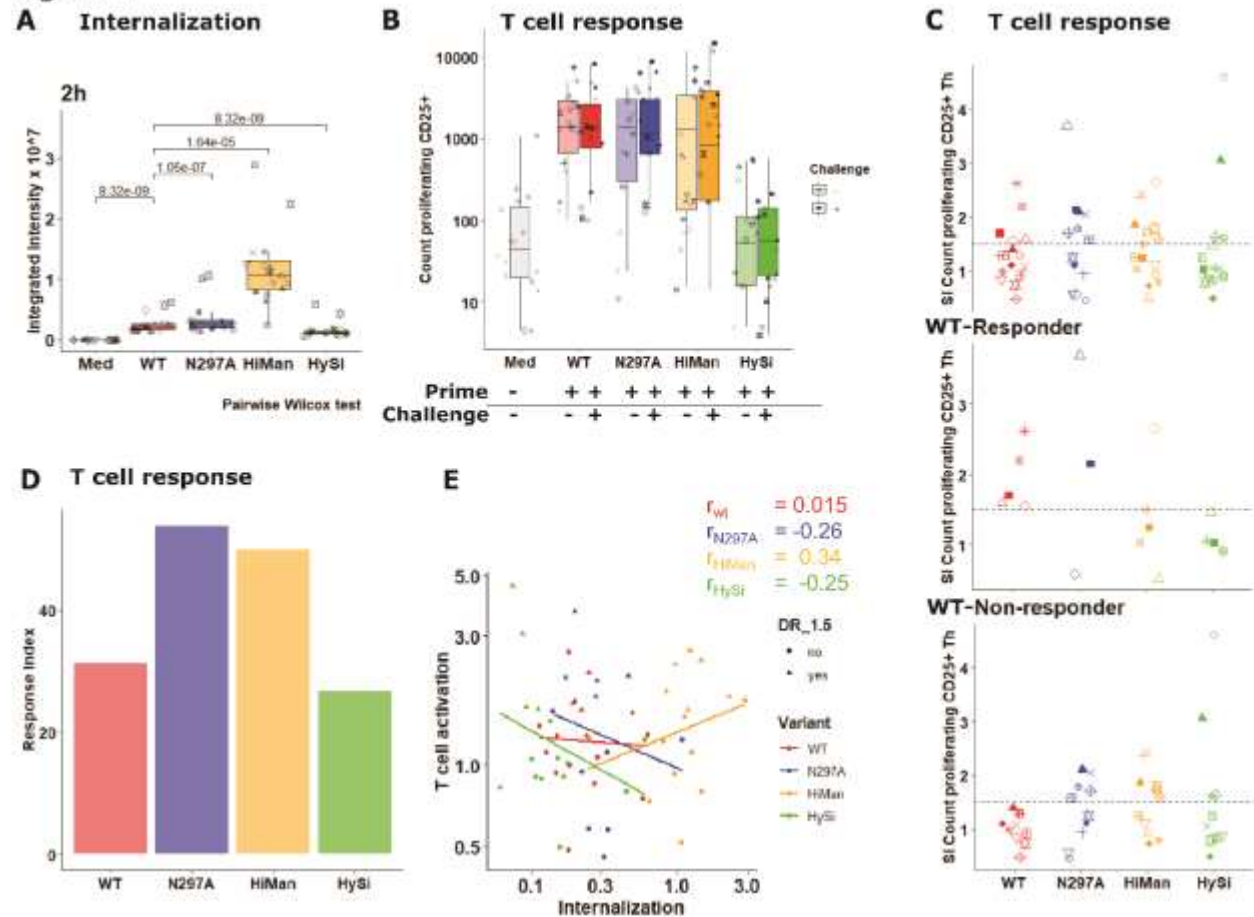
A: Theoretical lectin recognition motifs on rituximab (RTX) WT (unmodified) Fc N-glycans; AAL: *Aleuria aurantia* lectin (specific to core fucose), ConA: Concanavalin A (specific to $\text{Man}\alpha 1-6(\text{Man}\alpha 1-3)\text{Man}$), DSA: *Datura stramonium* agglutinin (specific to $\text{GlcNAc}\beta 1-4$), RCA: *Rhizinus communis* agglutinin (specific to $\text{Gal}\beta 1-4\text{GlcNAc}$); B: Binding of biotinylated lectins to RTX WT Fc N-glycans was assessed by ELISA: -Lec: Control without biotinylated lectin, aglycosylated (N297A) RTX served as negative control in addition to the medium control (Med); C: Competition ELISA with Methylmannoside (MM) for ConA and Galactose (Gal) for RCA; mean of technical duplicates of a representative experiment, error bars: SD

Figure 2**Figure 2:** Glycosylation facilitates and impacts binding and internalization by DCs

A: DC-internalization of unmodified (WT), aglycosylated (N297A), mannosylated (HiMan) and hypersialylated (HySi) rituximab (RTX) as measured by FACS at 60 min. % Internalization was calculated from the difference of the percentage of bound (4°C) and internalized (37°C) RTX on viable IDCs, $n = 6$ human donors, one data point represents the mean of technical duplicates, statistical analysis performed by pairwise Wilcoxon test; B: Target-binding of RTX glycovariants to CD20-positive Ramos cells is not affected by glycosylation, mean of technical duplicates from one representative experiment, Med: Medium control; Confocal images (40x) of IDCs from one human donor after binding at 4°C (C) and internalization at 37°C (D) of AF647-conjugated RTX glycovariants (red), nuclear stain: DAPI (blue); E: Quantification of intracellular RTX staining from confocal images as shown in D after DC uptake of RTX glycovariants at 37°C calculated with HALO™ image analysis software (Akoya Biosciences®), $n = 3$ images per variant from ~120 cells per image.

Figure 3**Figure 3: RTX glycosylation influences routing into the degradative pathway**

Images (40x) of immature dendritic cells (IDCs) from one treatment-naïve human donor after internalization of AF647-conjugated rituximab (RTX) glycovariants (red) co-localized with marker antibodies (green) for A: Lamp1 (lysosome), B: EEA1 (early endosome) or C: Rab7 (late endosome) detected by confocal microscopy; Quantification of co-localized RTX with respective endolysosomal markers calculated with HALO™ image analysis software (Akoya Biosciences®) from ~120 cells per image are shown right to the images. WT: unmodified, N297A: aglycosylated, HiMan: mannosylated, HySi: hypersialylated

Figure 4**Figure 4: Antibody glycosylation impacts T cell activation which is associated with internalization**

Internalization and T cell response was assessed in the same donor set. A: Internalization of rituximab (RTX) glycovariants by immature dendritic cells (IDCs) using the IncuCyte Real Time Imager (median from 13 - 16 human treatment-naive donors, Median Intensity: fluorescence signal derived from AF647-labelled RTX glycovariants indicating internalization) measured at 2h, one data point represents the mean of technical duplicates of one donor, statistical analysis performed by pairwise Wilcox test; B: Absolute count of proliferating (cells/mL) and CD25⁺ Th cells determined from PBMCs of 13 - 16 human treatment-naive donors (same donor set as in A) primed and challenged with of each the RTX glycovariant (10 μ g/mL); C: Stimulation indices calculated as ratio induced by the challenge relative to the prime response, donors were split into WT and non-WT responders; D: Response index for T cell assay in the same donor set, responding donor: donor with stimulation index above 1.5 (dashed line); E: Linear regression analysis for DC-internalization and T cell response induced by RTX glycovariants; WT: unmodified, N297A: aglycosylated, HiMan: mannosylated, HySi: hypersialylated

Figure 5

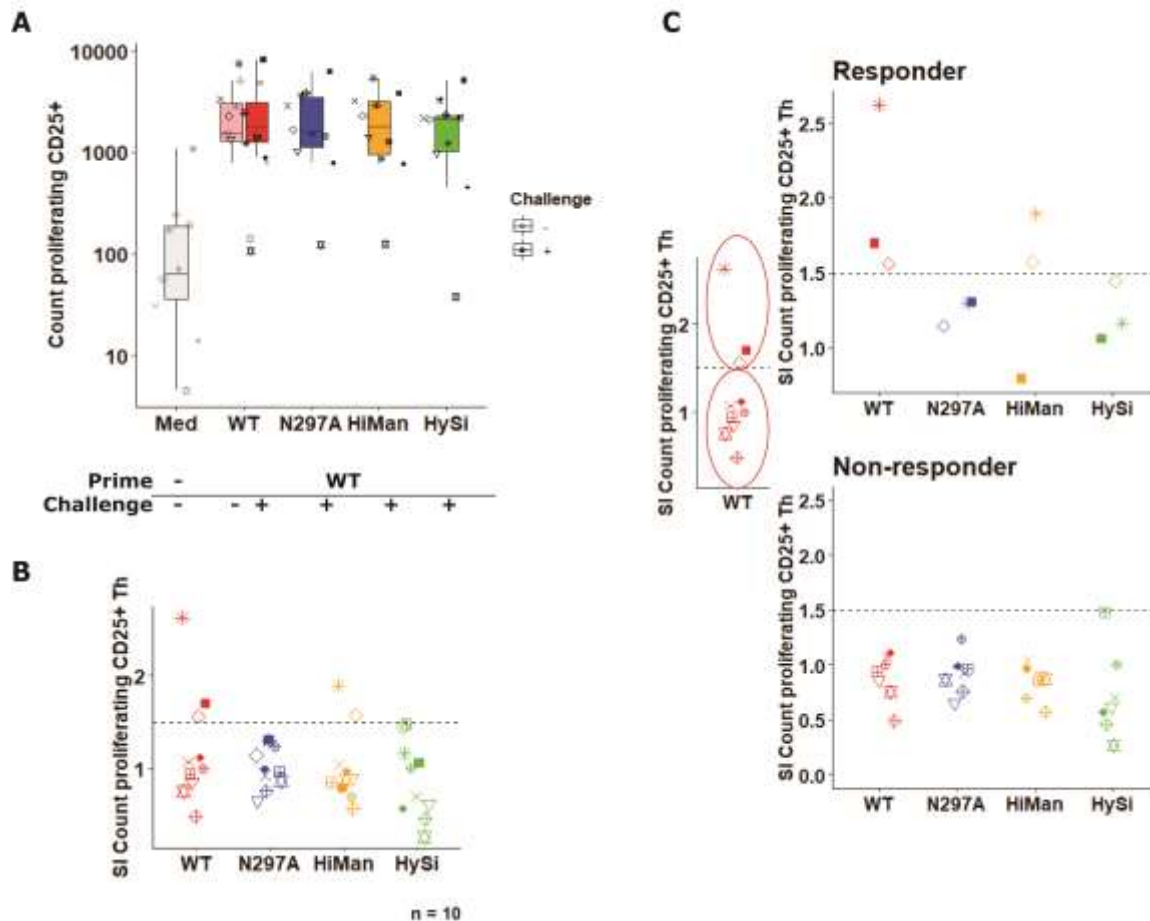
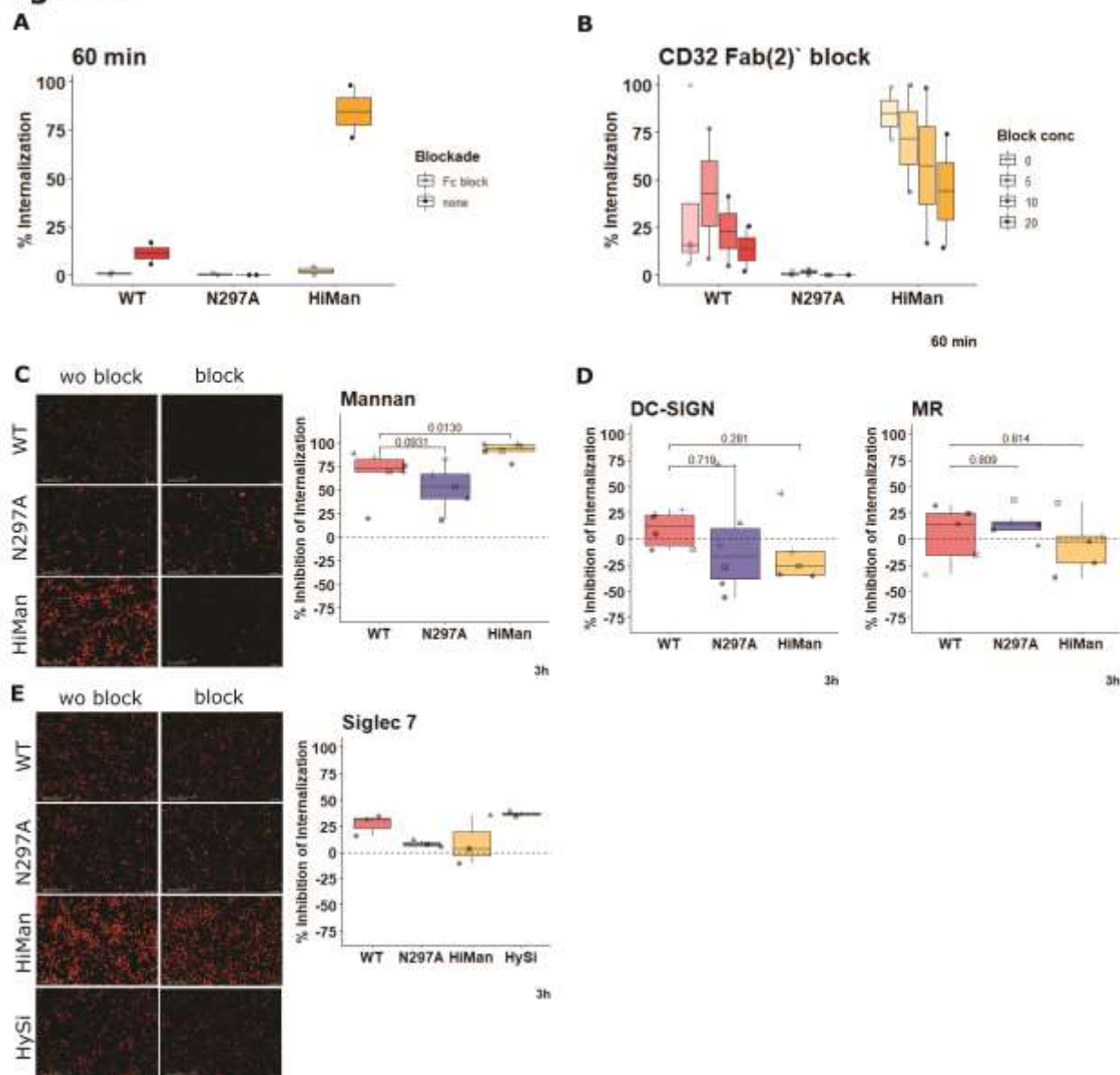
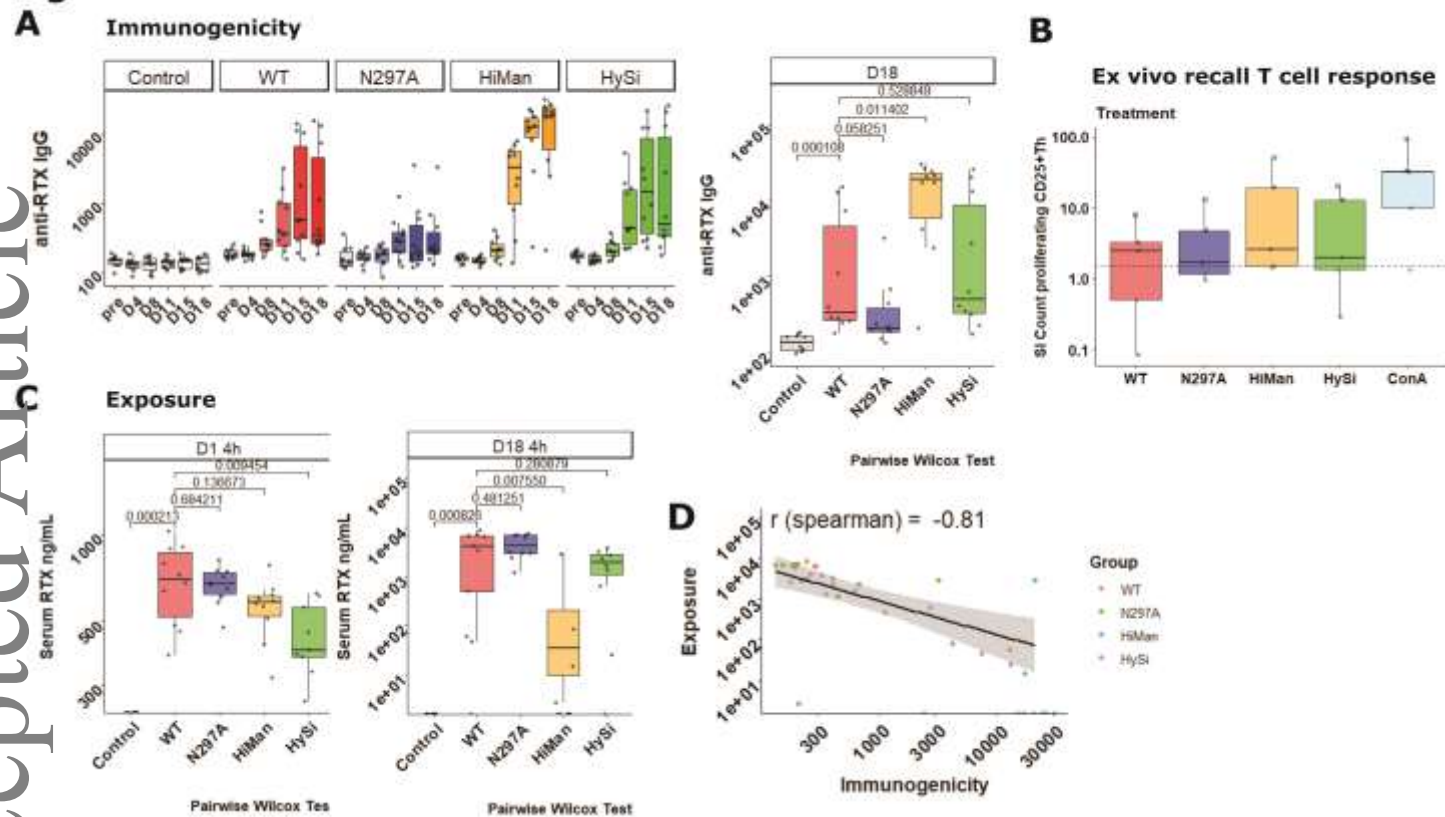


Figure 5: RTX glycosylation affects T cell recognition

A: Count of proliferating and CD25⁺ Th cells was determined from PBMCs of 10 human treatment-naive donors primed with WT RTX (rituximab) and challenged with RTX glycovariants (10 μ g/mL); B: Stimulation indices calculated as ratio induced by the challenge relative to the priming response; C: Tested naive human donors (n = 10) were split into WT and non-WT responders; WT: unmodified, N297A: aglycosylated, HiMan: mannosylated, HySi: hypersialylated

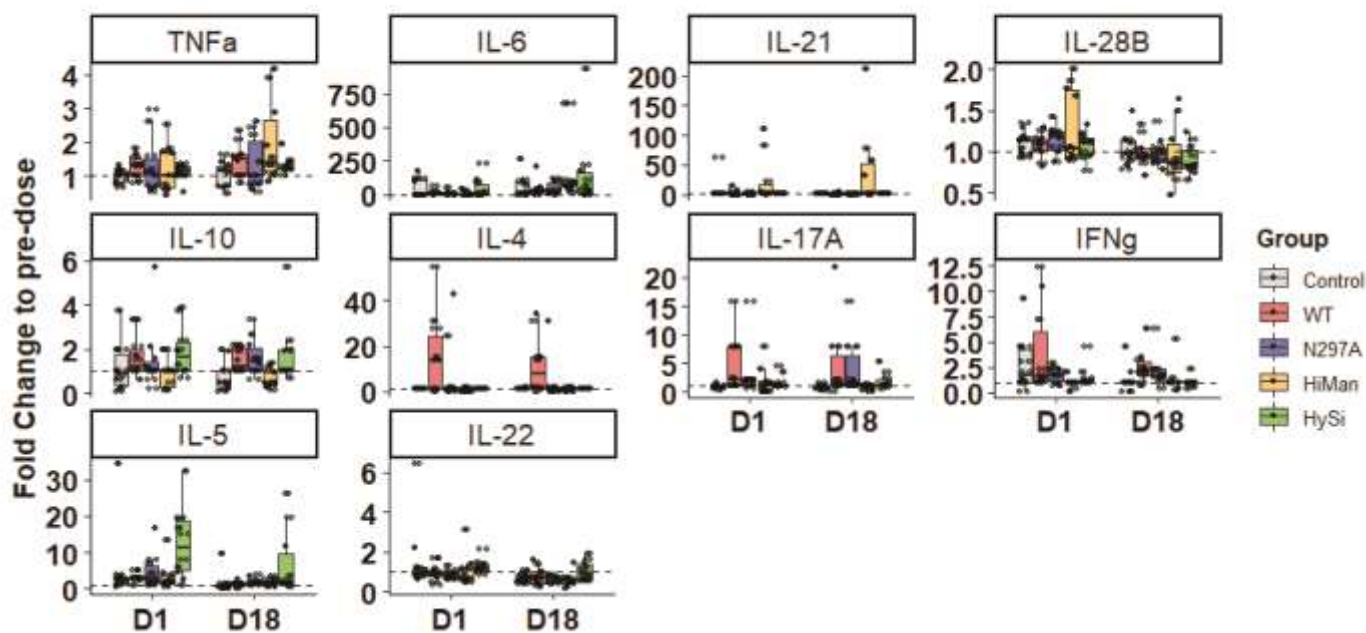
Figure 6**Figure 6: Fc γ R_s and LRs mediate glycosylation-dependent DC internalization**

Internalization of rituximab (RTX) glycovariants by immature dendritic cells (IDCs) determined by indirect FACS assay at 60 min in presence of A: full-length IgG, $n = 2$ donors, or B: CD32-directed F(ab) $_2$ at 5 – 20 μ g/mL, $n = 2$ donors; Inhibition of internalization of RTX glycovariants determined by the IncuCyte real time imager assay at 3h in presence/absence of C: 5 mg/mL mannan, $n = 5$ donors; D: 20 μ g/mL recombinant human DC-SIGN or 20 μ g/mL recombinant human CD206 (=MR), $n = 5$ donors. E: 20 μ g/mL recombinant human Siglec 7, $n = 3$ donors; F: Wo block: no ligand/recombinant receptor added, block: ligand or recombinant receptor added; numbers in the plots indicate p -values obtained from Tukey HSD; one data point represents the mean of technical duplicates of one donor; WT: unmodified, N297A: aglycosylated, HiMan: mannosylated, HySi: hypersialylated

Figure 7**Figure 7: Rituximab glycosylation impacts B and T cell immunogenicity and clearance in BALB/c mice**

BALB/c mice received 6 s.c. injections of 0.5 mg/kg rituximab (RTX) glycovariants or vehicle (Control) on D1, D4, D8, D15 and D18. Anti-RTX antibodies (ADAs) of IgG isotype determined in serum of A: BALB/c mice collected on D-13 (pre) and before s.c. injection of 0.5 mg/kg RTX glycovariants or vehicle control (Control) on D4, D8, D11, D15 and D18, $n = 10$ mice; ADAs after 6 doses of RTX glycovariants (D18); statistical analysis performed by pairwise Wilcoxon test; B: BALB/c mice ($n = 4$) were immunized by s.c. injection of 0.5 mg/kg RTX WT + alum or alum only (Control). Th cell activation and proliferation in the treatment group (immunized with RTX WT) after ex vivo recall of splenocytes with 1 $\mu\text{g}/\text{mL}$ of RTX glycovariant or 1 $\mu\text{g}/\text{mL}$ ConA; stimulation index (SI) calculated as ratio of the treatment (WT or ConA) to medium response, dashed line: response threshold at SI of 1.5; C: Serum RTX after 1 dose at D1 4h (left) and 6 doses on D18 4h (right). Statistical analysis performed by pairwise Wilcoxon test; one data point represents the mean of technical duplicates of one animal; D: Regression analysis on the relationship of

immunogenicity (anti-RTX antibodies) and exposure (serum RTX); WT: unmodified, N297A: aglycosylated, HiMan: mannosylated, HySi: hypersialylated

Figure 8**Figure 8: RTX glycosylation impacts cytokine response pattern in BALB/c mice**

Fold changes in serum cytokines determined on D1 and D18 4h post dose in BALB/c mice immunized by bi-weekly s.c. injections of 0.5 mg/kg RTX (rituximab) glycovariants relative to pre-dose, $n = 10$ mice, one data point represents cytokine results from technical singlicates from one animal due to serum volume limitations; WT: unmodified, N297A: aglycosylated, HiMan: mannosylated, HySi: hypersialylated